JOURNAL OF SPACECRAFT AND ROCKETS
Vol. 44, No. 4, July–August 2007

Solar Sail Structural Characterization Test Program

James L. Gaspar* and Thomas W. Jones†
NASA Langley Research Center, Hampton, Virginia, 23681
and
David M. Murphy‡
ATK Space Systems and Sensors, Goleta, California 93117

DOI: 10.2514/1.22897

The NASA in-space propulsion program sponsored intensive solar–sail technology and systems design, development, and hardware demonstration activities over the past three years. Efforts to validate an ATK Space Systems designed scalable solar sail system by functional demonstration in relevant environments, together with structural test-analysis correlation activities have recently been successfully completed. The tests spanned three phases of the program, with each phase lasting approximately 1 year; phase 1 focused on component tests of a mast segment and sail quadrant, phase 2 focused on a 10-m quadrant with two supporting masts, and phase 3 focused on a 20-m sail system with all four quadrants and masts. These tests were conducted for the purpose of validating analytical models that would be required by a flight test program to predict in-space performance. Specific tests included static shape testing using photogrammetry and modal vibration tests on the sail in a 1 torr vacuum environment using various excitation locations and techniques. The excitation methods were evaluated for their applicability to in-vacuum ground testing and their traceability to the development of on-orbit flight test techniques. The solar–sail masts were modal vibration tested in ambient atmospheric conditions and these results are also discussed.

I. Introduction

SOLAR sails are a very promising technology for a variety of space missions [1,2]. Over the past few decades, many disparate activities addressing elements of advancing solar–sail technology have been pursued. As a result, materials technology, fabrication experience, and applicable analysis technologies have been advanced to a point where projections for system performance have begun to have real credibility. Solar sails, especially as a system, present complex engineering challenges. In particular, the difficulty of validating structural modeling through rigorous testing in a fully representative environment before flight has thus far discouraged near-term mission planners from using this form of propulsion technology.

NASA has a particular interest in the maturation of solar–sail propulsion technology because this technology will enable or enhance a variety of road-mapped space science missions [1,2]. In 2001, the In-Space Propulsion (ISP) Program, managed by the Office of Space Science at NASA headquarters, determined that the time was right to pursue a system demonstration of sail technology that would elevate the technology readiness level (TRL) of solar sailing technology enough to allow flight implementation. NASA embarked on a competitive, multiyear program that was implemented by the ISP projects office at the NASA Marshall Space Flight Center (MSFC) to pursue the development and ground demonstration of system-level sail technology.

At the start of 2003, ABLE Engineering (now part of ATK Space Systems), under the purview of the ISP projects office at the MSFC, began developing scalable analytical tools and advanced design technologies for a solar sail system, which led to two follow-on phases for system ground demonstrator (SGD) development and validation. This joint effort, led by ATK, included the Systems Technology Group of SRS Technologies (sail assembly provider), the NASA Langley Research Center (LaRC) for sail shape and dynamics modeling and test execution, Arizona State University for attitude control modeling, Princeton Satellite Systems for sailcraft control software, and the MSFC Space Environmental Effects Laboratory for materials characterization and life evaluation.

The scalable square solar–sail (S4) SGD and validation activities were planned to systematically reduce the risk of flight implementation through building increasingly more complex solar–sail systems, together with the pursuit of high-fidelity analysis methods and testing of the highest fidelity possible in the terrestrial environment. Incremental design and demonstration was pursued to minimize cost and risk while methodically elevating the TRL of dependant systems before full-system demonstration. In phase 1 of the program (6 months), activities were focused on design and analysis refinement of the initial sail-system concept [3] and refinement of plans for hardware development and demonstration [4] to be conducted in phases 2 and 3. The phase 2 effort encompassed design, fabrication, and validation through a series of component and system tests [5] of a 10-m quadrant (one sail quadrant, two masts). The validation activities culminated with the demonstration of deployment, and sail shape and system-dynamics measurements [6] in vacuum at the LaRC in April 2004 [7]. In phase 3, a larger and more complete 20-m sail system was designed, fabricated, and demonstrated [8]. Tests included sail-assembly deployment trials at SRS, subsystem evaluations in ambient conditions at ATK before and during system integration and checkout, launch venting at Wyle Laboratory, vibration testing at Environment Associates, and finally, system deployment, functional demonstrations, and shape and dynamics measurements at the 100-ft-diam thermal-vacuum chamber at NASA John H. Glenn Research Center (GRC), Plum Brook Station, in April and May 2005 [9]. The 20-m hardware represents a flight-worthy full system with four sail quadrants, and four masts, an instrument offset boom, additional dual-purpose mechanisms for deployment and attitude control, tiedown and release hardware, solar panels, and launch vehicle interfaces. This system is integrated together in a carbon-fiber-reinforced composite central assembly that also functions as a bus chassis [10].

Several lessons were learned in the development of test methodologies for the subsystem hardware on the 10-m quadrant that

Received 31 January 2006; revision received 31 January 2007; accepted for publication 31 January 2007.

*Research Engineer, Structural Dynamics Branch. Member AIAA.
†Research Engineer, Advanced Sensing & Optical Measurements Branch. Member AIAA.
‡Chief Research Engineer, Solar Arrays and Deployables. Member AIAA.

were integrated into the test activities supporting the construction and testing of the full sail system. The objective of the present study is to describe the evolution and integration of these test technologies into the 20-m sailcraft validation program. In particular, the paper describes the results of sail subcomponent, 10-m quadrant, and 20-m system-test validation activities; as well as a description of lessons learned and recommendations for follow-on flight test programs. To accomplish the objectives of the current study, the hardware is described first. Then, a description of the dynamic testing is presented for each test article. And finally, a description of the static shape testing completed on the 10-m quadrant and 20-m system is presented.

II. Hardware and Test Program Development

The S4 hardware subsystems were designed and demonstrated incrementally in the three-phase ISP program, and the lessons learned from each phase were incorporated into subsequent development activities. Phase 1 included the development of two engineering development unit (EDU) masts and a number of sail subassemblies. In phase 2, longer masts and a refined sail assembly were built and integrated together into a 10-m deployable quadrant of a symmetric sail system. It was left to the third phase of the program to develop a full flightlike, four-quadrant, 20-m sail system included with a carbon-fiber-reinforced composite central structure, and the addition of other mechanisms such as actuators. These phase 3 advancements, together with larger, lighter sails and longer masts, allowed the S4 sailcraft system to be completely demonstrated. The design features and evolution of the mast and sail hardware test articles through the phases of the program are discussed in this section. The progression of the major hardware elements that were tested is shown in Fig. 1.

A. Masts

Because the sail is a membrane, the mast is a critical component that transfers pressure loads from the sail to the spacecraft center of mass. For this reason the design for the masts, in the first phase of the program, were developed from an advanced version of the continuous coilable structures that ABLE has flown 27 times in space with 100% success. By using a graphite coilable design, the mast incorporated design advances that provided a minimum-mass configuration ideal for these ultralightweight systems. An initial EDU of an ultralightweight carbon coilable mast was constructed using off-the-self composite materials, because the program focus was on new gossamer concepts for the structural joints along the longeron, at the interface of the battens and diagonals. This first EDU, a ten-bay mast, was sent to the LaRC as part of the effort to develop and evaluate dynamic-excitation test techniques. A second EDU (also a ten-bay mast) was built with fittings derived from flight-heritage masts, but sized much smaller and composed of a magnesium alloy. This mast also demonstrated new custom-pultruded longerons and battens made of graphite–epoxy composite material. The functional validation of this new gossamer sail mast design provided confidence to proceed with the fabrication of the two 7-m (31-bay) masts needed for the 10-m quadrant assembly to be used in the second phase of the program. This basic mast design used in phase 2 of the program was used later to develop the 20-m system used in the third phase of the program. Thus, the results obtained in the development of the second EDU examined in phase 1 and the 7-m mast testing conducted in phase 2 directly influenced the development of the 14-m masts tested in phase 3 of the program for the 20-m system.

B. Sail Membranes

In phases 1 and 2 sail development efforts, which paralleled the development of the EDU masts, SRS Technologies began developing fabrication equipment and assembly processes for the thin-membrane sail materials. The sail material, denoted by CP1 (clear polyimide 1), is a polyimide material developed by the LaRC and produced under exclusive license by SRS Technologies. This material has had significant space environment exposure, in both real and simulated environments. The material has been flight qualified for a 15-year exposure in a GEO (geostationary orbit) environment. For this application, the sails built were all configured as triangular "quadrants" with scalloped edges that attached to the sail masts at each corner. A strong motivation behind the selection of a three-point-attachment configuration was to ensure planarity, regardless of intrasail optical or mechanical anisotropy, system orientation to the sun, or thermal cycling. The border scallops are trimmed with a high-strength graphite cord that imparts robustness for handling and

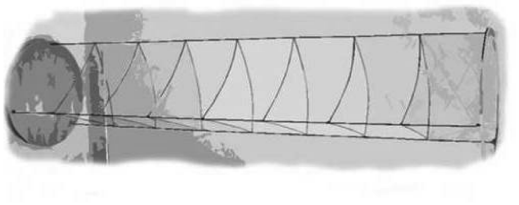

a) EDU mast

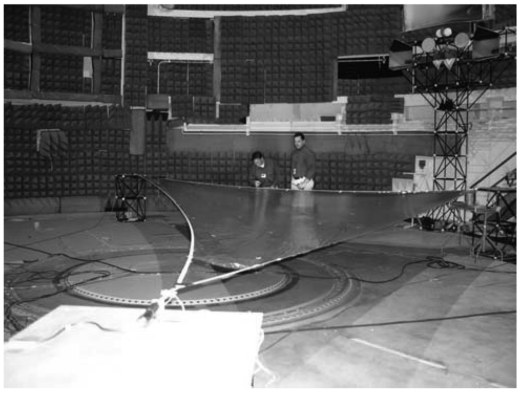

b) 10-m sail quadrant component (no masts)

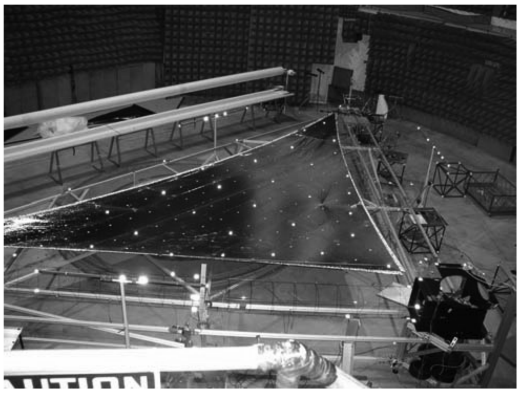

c) 10-m system (1 quadrant and 2 masts)

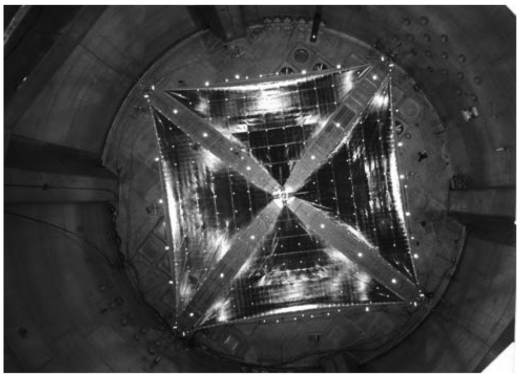

d) 20-m system (4 quadrants and 4 masts)

Fig. 1 Progression of major hardware builds.

deployment. Inboard of the cord, was a corrugated border area that allows thermal and mechanical strain decoupling to the main sail. These features provided uniform membrane stress to ensure predictable shape and high propulsive efficiency. After several iterations of their concept, SRS provided a refined sail measuring 5 μm in thickness, denoted as RS5 (refined sail 5 μm), and another sail that was incorporated with a 3 μm film, denoted as RS3 (refined sail 3 μm). LaRC personnel used both of these sails in component- and system-level (10-m quadrant) tests to validate the corresponding analytical models.

C. 10-m System

After completion of the mast and sail subassembly validations in phase 2, the subassemblies were integrated into a 10-m quadrant assembly. To validate deployment characteristics, sail shape, and system dynamics, a series of tests were planned using the LaRC 16-m vacuum chamber facility at 1 torr. Testing in a vacuum was necessary because both the dynamics of the deploying and deployed sail would otherwise be greatly affected by the surrounding air mass. For example, the air mass within 2 mm of either side of the sail surface equals the mass of a 3 μm sail film. The priorities for testing were first, to validate deployment; second, to measure the deployed shape of the (horizontal) sail billowed under gravity loading; and third, to validate analytical models for system dynamics. The ATK and LaRC test team planned an extensive series of tests to capture the data needed to support these priorities, as well as to meet goals for developing test methods applicable to 20-m sail testing and to in-flight investigations of larger-scale systems.

D. 20-m System

The primary formal tests for S4 demonstration and validation were performed at GRC, Plum Brook Station. This facility is a 100-ft-diam thermal-vacuum chamber. The priorities for this activity were to demonstrate deployment robustness, and to obtain sufficient shape and dynamics data required for validation of the analytical models [11]. Three full-system validation deployments were completed. The first deployment was in ambient conditions, the second in a vacuum, and the third (also in a vacuum at 10×10^{-5} torr) with a thermal gradient imposed across the stowed system. During the third deployment, an intervention was required to correct a simple integration error that led to a halyard entanglement. Otherwise, the three deployments were successful. The key analytical validations for the 20-m system paralleled the activities performed on the 10-m quadrant in phase 2, namely, shape and dynamic-response characterization. Shape data were obtained to study the magnitude of mast droop and sail sag caused by gravity. LaRC personnel employed five photogrammetry cameras to measure the system at three spreader-bar positions (the nominal and the two extremes). To capture dynamic-response data, LaRC personnel used both external inputs and response sensors to measure the first few modes and modal frequencies of the system. In addition, embedded actuators and sensors that are applicable to a flight program were used. The shape and dynamic-response data obtained compared well with pre-test-analysis predictions. A review of the testing for dynamics and static shape during each phase of the program is given subsequently.

III. Dynamic-Response Testing

A. Measurement Methods

A scanning laser vibrometer system was the main instrument used to measure the vibration modes for all the test articles, throughout all three phases of the test validation program. To provide accurate measurements, retroreflective dots were adhered to the sail and mast test articles, typically in an evenly spaced grid pattern. These retroreflective dots are used to enhance the reflection of the laser beam to the laser vibrometer. For vacuum tests, a pressurized canister was fabricated to place the scanner inside to protect the delicate laser scan head from the vacuum environment. The canister has a window port that permits the laser scanner to view the test article. A temperature sensor inside the canister was controlled by a switch that would automatically shut the scan head down at 100°F to prevent overheating. Forced air flow was used to cool the inside of the canister. For the sail-only component and the 10-m quadrant tests completed in vacuum, the vibrometer was hoisted with cables and carefully centered approximately 50 ft directly above the test article to enable the required scan range.

In planning for the 20-m sail test at the Plum Brook facility, it was found that due to insurmountable limitations on the maximum length allowed for the vibrometer scan head cable (30 m), the vibrometer cable was not long enough to allow for positioning the instrument directly overhead of the test article. After an extensive investigation of alternate techniques to enable scanning the entire test article with the laser, the following configuration was selected. The vibrometer test configuration consisted of the vibrometer canister mounted on the chamber door ledge and oriented so that the laser beam points up toward the center of the domed ceiling of the chamber. Near the top of the chamber ceiling is a crane structure, which is centered directly above the test article (about 30 m). This crane structure was used to mount an active scanning mirror system (SMS) that was designed to receive the laser beam from the vibrometer and redirect it toward the test article below for dynamic-response measurement. This configuration is illustrated in Figs. 2 and 3. The SMS system was composed of two mirrors mounted on galvanometer motors and oriented orthogonal to one another to enable two-axis scanning with a range of ± 20 deg. The galvanometer motors have similar pointing

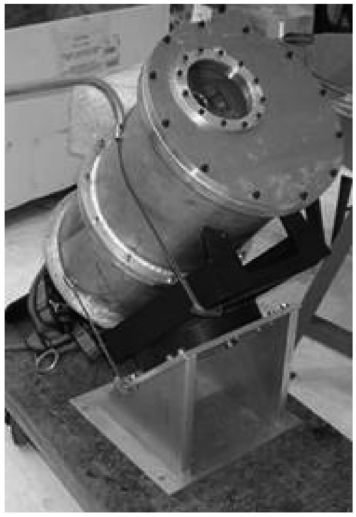

a) Vibrometer inside canister

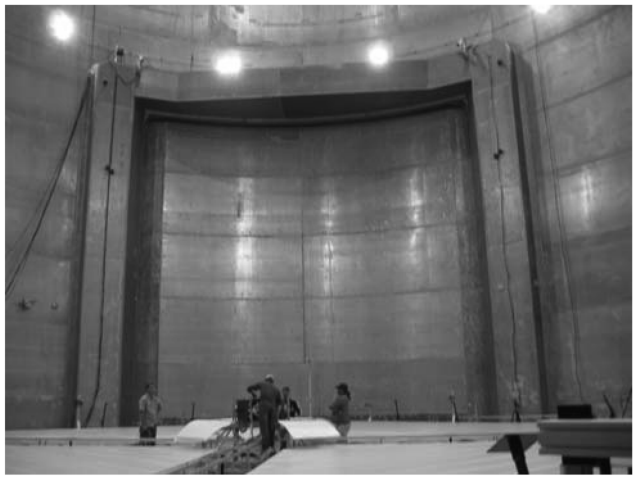

b) Inside of vacuum chamber

Fig. 2 Instrumentation inside vacuum chamber for 20-m system.

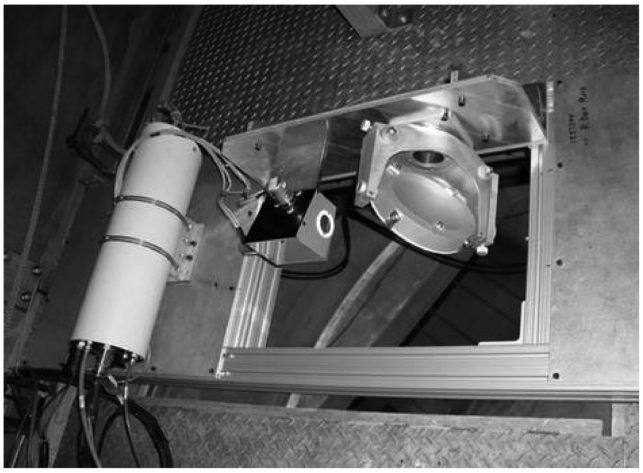

Fig. 3 Scanning mirror system inside vacuum chamber for 20-m system test.

accuracy specifications to those used in the vibrometer scanner system, which allows for precision target tracking from large distances. A specially developed target tracking algorithm enabled automatic centering of the laser beam on each retroreflective target to be measured. Before this test, the vibrometer scanning system was validated to work at an 85-m range (although larger distances are possible), well beyond the required working distance of 60 m for the configuration used in the present study.

B. Mast Results and Discussion

Mast-tip dynamic-response measurements were obtained using the laser vibrometer in ambient conditions on the EDU mast, on both 7-m masts of the 10-m quadrant, and on each of the four masts of the 20-m system. The laser vibrometer was configured to measure the vertical responses of the two upper longerons that are adjacent from one another at the mast tip. The lateral motion of the lower longeron was measured using a mirror to redirect the laser, as seen in Fig. 4. By comparing the phase of the three responses measured at the mast tip from the frequency response function (FRF) data, it was possible to determine if the mode was dominated by longitudinal bending, lateral bending, or torsion.

Various mast excitation techniques were used during each phase of the test program to evaluate the most promising methods as the program matured. For the EDU mast, dynamic-excitation results were determined with a traditional impact-hammer method and compared with results obtained using a unimorph macrofiber composite (MFC) piezoelectric actuator. For the impact-hammer method, the test article was excited using a Piezotronics impact hammer, which was triggered by a digital-timer switch box for automated excitation. The hammer was secured to a heavy steel plate set on a platform that was positioned on a corner edge of the mast, as shown in Fig. 5. In this configuration, the impact hammer provides a consistent excitation input force that induces an out-of-plane disturbance on the mast. Note that the mast has been mass loaded to reduce its natural frequencies to a level more realistic for a much larger sized mast appropriate for a sail. The FRFs from this test were computed using six ensemble averages and 6400 frequency lines from 0–100 Hz. The other actuation method used ceramic-fiber-based piezoelectric MFC patches bonded to the long narrow longerons near the mast root. A periodic chirp signal was used with a frequency bandwidth of 0–70 Hz. The FRFs were computed using three ensemble averages and 4480 frequency lines from 0 to 70 Hz. As shown in Fig. 6, the forward two piezoelectric patches are activated out of phase with the back patch to induce bending vibration near the mast root. The dynamic-response results obtained for the EDU mast by the patch-actuator excitation were very encouraging. It was observed that the actuators could effectively identify the first two mast modes, including torsion. The actuators reacted against a very stiff longeron and required only a small surface

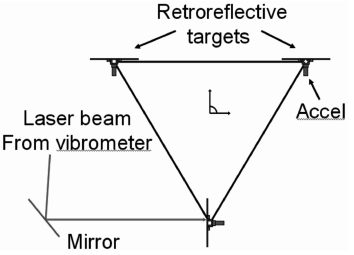

Fig. 4 Measurement targets on mast tip for all mast testing.

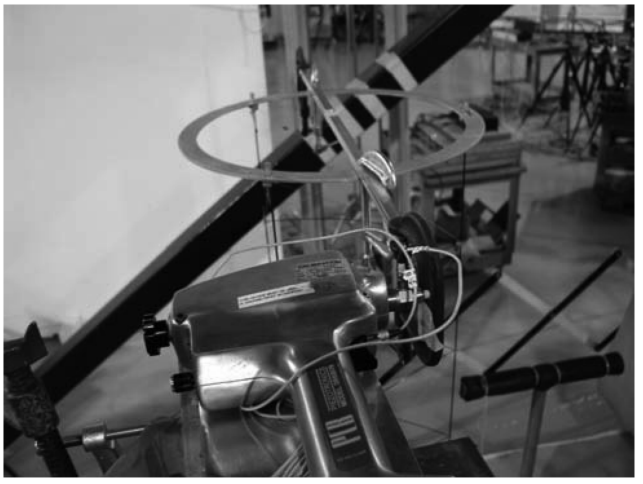

Fig. 5 Impact hammer at EDU mast tip.

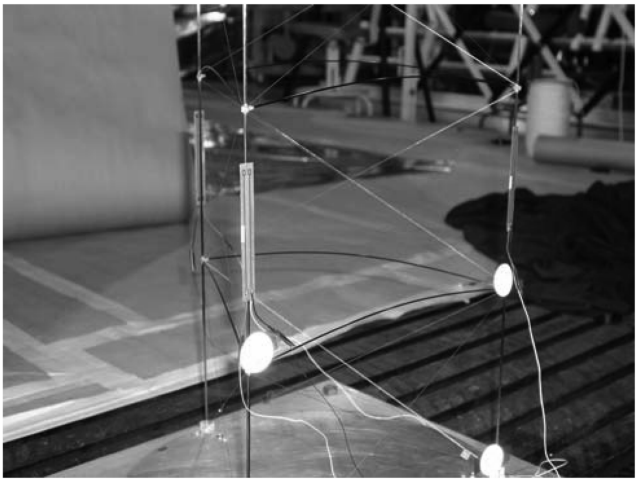

Fig. 6 MFC actuators on EDU mast.

area for bonding. The results from the piezoelectric patch-actuator test also corresponded very well with those obtained using the impact-hammer method, a more traditional modal-testing technique. Based on the success of the unimorph actuator for mast excitation, it was decided to investigate this technique further during the tests of the masts on the 10-m quadrant.

For the dynamic-response tests conducted on the masts of the 10-m quadrant system, traditional electrodynamic shakers were used as the baseline excitation technique. For these tests, the mast tips were unsupported, which allowed the masts to droop under gravity load. Each mast was excited near the root with an electrodynamic shaker that was mounted to excite lateral and torsion modes and then reconfigured to excite the vertical modes, as shown in Fig. 7. Dynamic response was measured at the mast tips, which were configured with accelerometers and retroreflective targets (Fig. 7d)

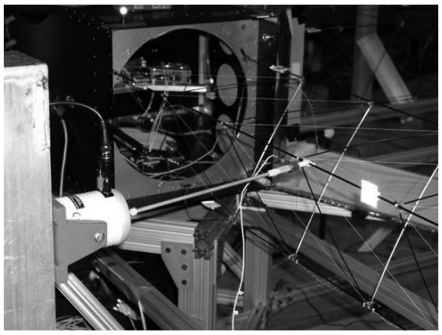

a) Lateral shaker attached to upper outer longeron of mast

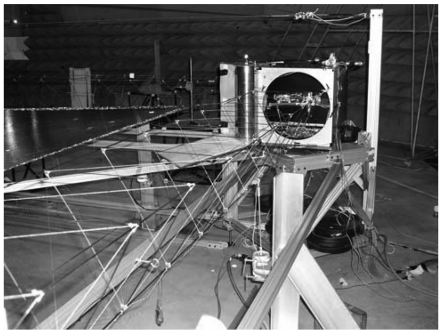

b) Vertical shaker attached to lower longeron of mast

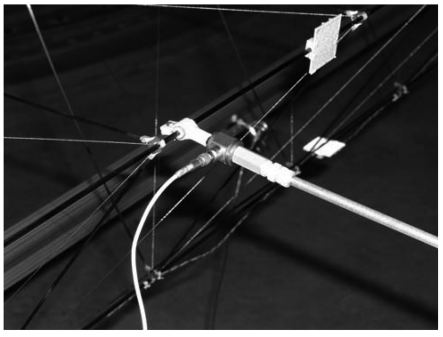

c) Stinger and load cell adapter for mast longeron

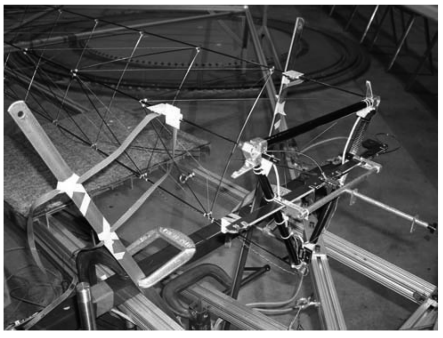

d) Vibration measured at mast tip with laser and accelerometers

Fig. 7 Mast excitation with shaker for 10-m system.

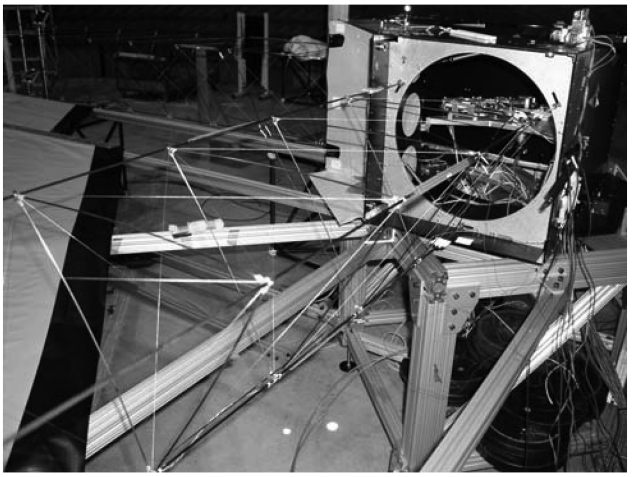

a) MFC on each longeron at bay 3

b) MFC bonded to upper longeron in a plane 45 deg from vertical

Fig. 8 MFCs near mast root on 10-m system.

for laser vibrometry. The excitation was provided in the form of a sine-wave sweep from 3.5–8.5 Hz, with five averages used to compute the FRFs. The other actuation method in these tests used ceramic-fiber-based piezoelectric patches bonded to the long narrow longerons near the mast root, as shown in Fig. 8. The excitation was provided in the form of a sine-wave sweep from 3.5–8.5 Hz, with five averages used to compute the FRFs. To excite a vertical mast response, the two patches on the upper longerons were driven in-phase with one another to induce vertical bending vibration near the mast root. Then, to excite a lateral mast response, the two patches on the upper longerons near the mast root were driven out of phase with one another to induce lateral bending vibration modes. This directional control of the mast vibration was achieved by mounting the patches diagonally on the longerons, such that they produce a component of excitation both in the vertical and lateral directions. When driven in-phase, the net mast response in the lateral direction is diminished (the two patches react against one another), while on the contrary the vertical component is enhanced (the two MFCs work together to induce vertical motion). When driven out of phase, the patch-actuator excitation enhances the lateral-motion component and diminishes the vertical motion. In both cases, the patch-actuator concept was able to produce visible motion at the mast tips in either the vertical or lateral directions. The patch actuators were shown to work very well, even though this mast was much longer than the EDU mast. Results are presented in Fig. 9 that show the modes were very well excited with good coherence at resonance. The patch-actuator dynamic-response results matched well with the corresponding results obtained from the baseline shaker tests. However, it should be noted that the x-mast frequencies are consistently lower than the y-mast results (Table 1), which is attributed to the two loose diagonal wires at the root on the x mast. Gravity loading of the mast tends to off load these diagonals; in this case, the x mast was off loaded more than the y mast.

The dynamic-response tests for the 20-m masts were performed in ambient atmospheric conditions with the mast tips off loaded with a long-cable system (without a negator spring). This system was designed by ATK and included in the analytical models used to allow

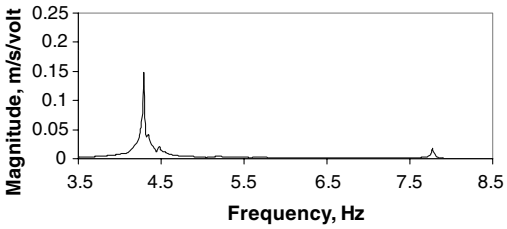

a) FRF, excited in-phase

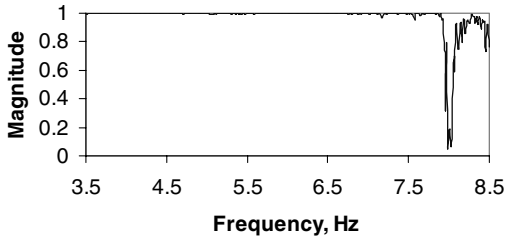

b) Coherence, excited in-phase

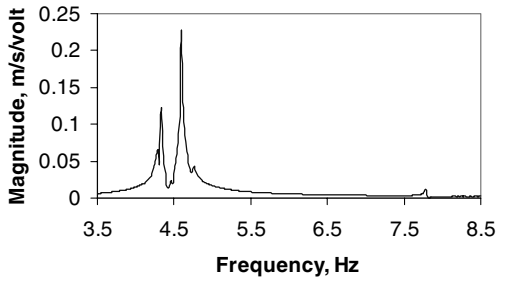

c) FRF, excited out-of-phase

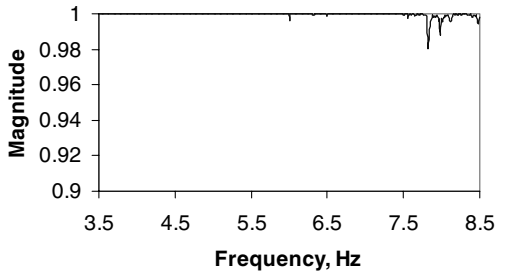

d) Coherence, excited out-of-phase

Fig. 9 Mast tip response from MFC excitation on 10-m system.

for correlation with the test results. Shakers were ruled out as a baseline excitation technique, because of major time constraints and the difficulty with installing shakers on a fully deployed system. The piezoelectric patch actuators that worked so well on the 10-m quadrant were also ruled out, because it was determined that high strains are likely to be present in the longerons, while stowed, that could decharge or damage the brittle piezoelectric fibers. Further study, and hence additional time, would be required to validate the actuators for this high-strain loading. Instead, the baseline excitation method used in the dynamic-response tests was a piezoelectric stack actuator excitation located at the mast root. ATK Space Systems had preintegrated piezoelectric stack actuators positioned in-line with each longeron at the mast root, as shown in Fig. 10, for the purpose of obtaining the dynamic responses of the mast. This actuator excitation configuration is a strong candidate for on-orbit flight testing because it is easily incorporated into the sail design, and it is considered the baseline test to which the finite element (FE) analysis results are to be correlated. It was found that one actuator located on the upper longeron could provide enough force to excite the longitudinal, lateral, and torsion modes of vibration. Therefore, all the masts were tested by driving just one upper longeron. The response was measured at the mast tip in the vertical direction at the two upper longerons, and in the lateral direction at the lower longeron. All mast tests applied a sine-wave sweep input signal to the exciter with a bandwidth from 0 to 10 Hz. The FRFs were computed using the input voltage as a reference value and using four averages. By comparing the phase of the three responses at the mast tip obtained from the FRF data, it was possible to determine if the mode was dominated by longitudinal bending, lateral bending, or torsion. Figure 11 shows the vertical and lateral response for the $+y$ axis mast tip. The FRFs and coherences obtained from all the mast tests were excellent, with very well-defined modal peaks and good coherence across the entire frequency spectrum. The consistency of the mast responses was

Table 1 Vibration modes of masts for 10-m system using shaker excitation

	Frequency		Description
Mode, #	*x* mast, Hz	*y* mast, Hz	Operating deflection shape, ODS
1	4.30	4.36	First lateral bending *x* and *y* mast in-phase
2	4.39	4.40	First vertical bending Mast phasing not identified
3	4.56	4.63	First lateral bending *x* and *y* mast out of phase
4	7.35	7.78	First torsion Mast phasing not identified

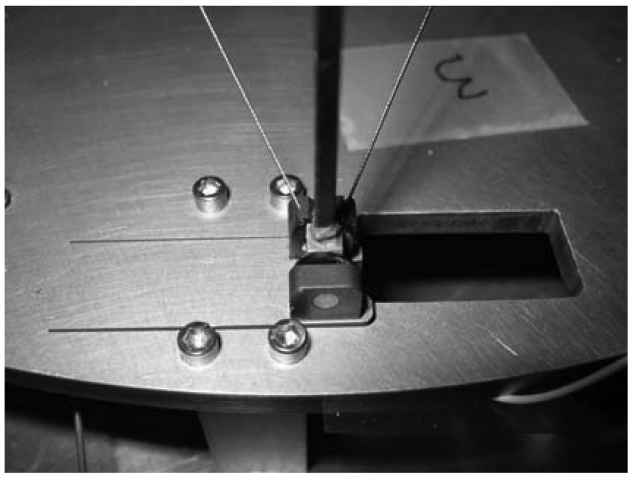

a) Base plate flexure allows axial displacement of longeron via piezoelectric stack

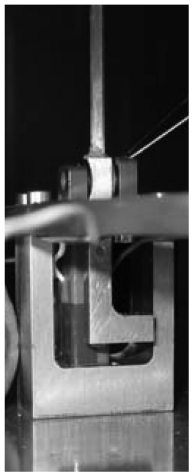

b) Longeron load path runs through base plate flexure into actuator

Fig. 10 Excitation at mast root with in-line longeron actuation for 20-m system.

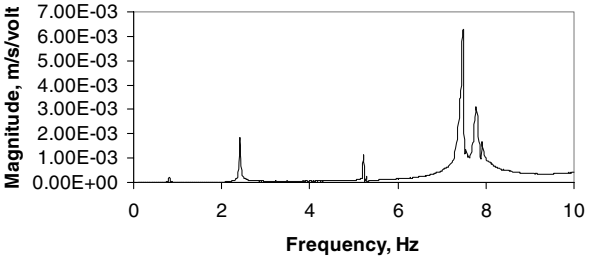

a) FRF vertical

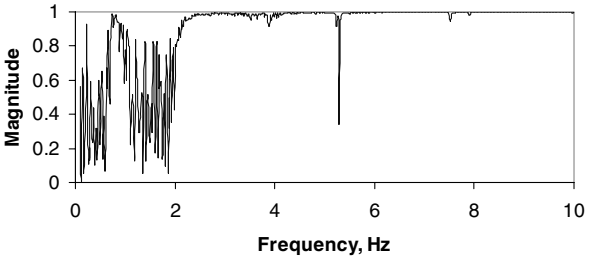

b) Coherence vertical

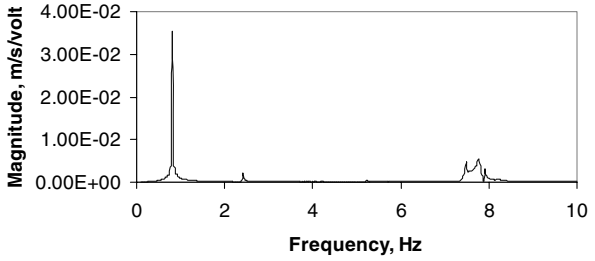

c) FRF lateral

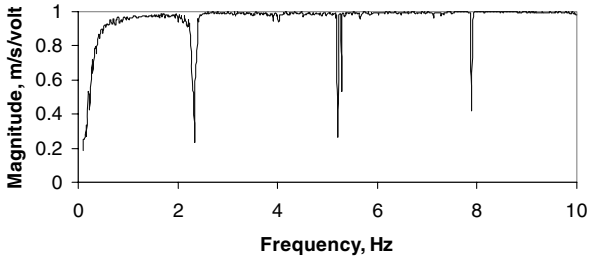

d) Coherence lateral

Fig. 11 Mast tip vertical and lateral response measurements (+*y* mast) 20-m system.

excellent (see Table 2), with all four masts exhibiting almost identical responses for all the fundamental modes. Thus, the piezostack excitation at the mast root was very successful. This technique not only saved valuable testing time, as no setup was required, but is also applicable to flight testing.

C. Sail Results and Discussion

The baseline excitation technique used for all the sail dynamic-response tests (i.e., sail-only component, 10-m system, 20-m system) conducted in a vacuum consisted of using electromagnets to excite the three corners of the sail membrane. The magnetic excitation method is a noncontact technique where an electromagnet is used to provide out-of-plane motion to the sail by moving a small strip of metal fixed to the sail corners [12]. The magnets were driven with a slow sine-wave sweep and various combinations of magnets would be active during a test to excite the lowest-order modes. The sail-only component and 10-m system tests used only magnets positioned at the three corners for sail excitation. The 20-m test included additional magnets positioned along the hypotenuse of each sail quadrant to excite modes that are difficult to excite using magnets placed at the sail corners. A second excitation technique that was used for all in-vacuum dynamic-response tests consisted of ceramic fiber-based piezoelectric patches applied to the edge region of the sail (normally referred to as a cord). The ceramic-based patches were developed at LaRC and are denoted herein by MFCs [13]. Similar actuators have been demonstrated to work on smaller scale membranes in previous experiments. Actuators were placed at various positions on the membrane to determine their capability for exciting the membrane modes. A bimorph MFC configuration was required, in which two MFCs are bonded to each other and driven out of phase to induce an out-of-plane motion. Unlike the magnetic exciter, which is noncontacting, the MFCs are bonded to the top surface of the sail cord region with double-backed adhesive transfer tape. Strain-gage wires are soldered to the MFC leads. For all tests performed, the actuator wires were carefully secured to minimize their effect on the sail-membrane vibrations. The surface-bonded bimorph MFC configuration provides a small out-of-plane disturbance on the membrane due to the bending caused by the shear force created at the interface between the two MFCs when driven out of phase with high voltage. This bending can be seen as a small bulge on the surface of the membrane at the actuator location. The out-of-plane disturbance is capable of exciting the vibration modes of the structure when the actuator is strategically positioned on the membrane. Piezoelectric patches are most effective when placed at strain antinodes, that is, the strain in the direction of the actuator is high. This position is different from what is used during a traditional shaker modal test, where the shaker is most effective at the displacement antinodes. During the sail-only component tests, many actuator locations were evaluated for their effectiveness at exciting sail modes. These actuator patch locations, shown in Fig. 12, included excitation near the corners as well as at the center cord region of the sail.

The first four dominant mode shapes obtained by using a single magnetic exciter positioned at the 90-deg corner of the sail, referred to as the tack line, are shown in Fig. 13 (test configuration 1). The corresponding FRF and coherence plots in Figs. 13e and 13f show that all four of the modes are excited well with smooth symmetric mode shapes. The few low coherence values occur near antiresonances, where the signal-to-noise ratio is poor and low coherence is acceptable. The mode shapes also correspond well with those predicted by finite element analysis. Test configuration 2 uses actuation by MFCs at the right-angle corner location near the tack line. Figure 14 shows that the first two modes were excited well, with good coherence. These modes also corresponded well with analysis predictions. In this case, the frequencies are somewhat higher due to

Table 2 Mast dynamics test summary

#	Mode description	Frequency comparison, Hz			
		$+y$ mast	$-z$ mast	$-y$ mast	$+z$ mast
1	Mast bending in horizontal plane	0.813	0.813	0.797	0.797
2	Mast twist	2.41	2.39	2.41	2.39
3	Mast bending in vertical plane ($-z$ mast)	——	5.14	——	——
4	Mast bending in vertical plane	5.22	5.23	5.27	5.30
5	Mast bending in vertical plane (some twist on $-z$ mast)	7.47	7.50	7.55	7.50
6	Mast second bending (only mast tips measured)	7.75	7.84	7.75	7.84

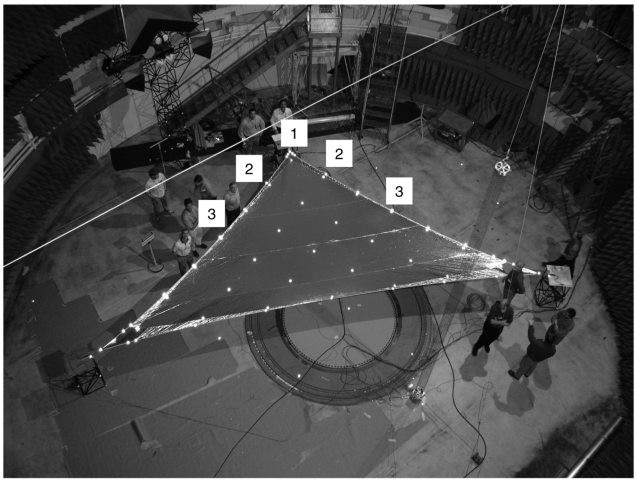

Fig. 12 MFC actuator locations for 10-m sail component testing.

the higher halyard-corner load of 5 lb. Test configuration 3 uses the MFCs at the short cord center for actuation. Figure 15 shows that the third mode was excited well when the actuators are activated in-phase with one another, whereas the fourth mode is well excited when the two actuators are driven out of phase. This difference can be expected, because the in-phase actuators are exciting the symmetric modes and the out-of-phase actuators are exciting the antisymmetric modes.

Based on the success of the magnetic and MFC actuation techniques demonstrated during the component tests, the techniques were used again for the 10-m quadrant dynamic-response test. Using electromagnets at the sail corners as the baseline excitation method, the first four sail-membrane modes were properly identified with very strong FRFs and high coherences at resonance, as shown in Figs. 16 and 17. In addition, Fig. 18 shows that the mode shapes are smooth and symmetric, and these modes correspond with those found during sail-only tests. The first, second, and fourth modes were all obtained with two magnets placed at the halyard corners and driven out of phase with one another, with a slow sine-wave sweep. The third mode was obtained in a separate test with only the magnet at the tack line active (shown in Fig. 18) during the sine-wave sweep. Modes for the 10-m quadrant were also obtained using the same bimorph MFC concept demonstrated earlier during phase 2 on a sail-only component. Except, in this case, the MFC design had been made narrower to better fit on the sail cord, which had been made thinner during a design modification. Figures 19 and 20 show that a single MFC bimorph actuator positioned on the cord, near the sail central hub, was able to excite the first three sail-membrane modes very well.

The dynamic response of the 20-m system was evaluated for a single nominal sail tension that corresponds to approximately a 2.5-lb halyard load (near mast tip), and for a baseline 0-deg spreader-bar angle (sail rotation at mast tip), and a spreader-bar angle that is 22.5 deg from the horizontal direction. Both of the movable ballast masses of the attitude control system (ACS) were stowed inside the central assembly during dynamic-response testing. The baseline excitation method for the tests used electromagnets mounted at each corner of the sail-membrane quadrant. A total of 12 magnets were precisely aligned at the corners of each sail (three magnets per sail quadrant), configured as shown in Fig. 21a. In addition, magnets were positioned on the long cord at the center of the hypotenuse of each sail quadrant, as shown in Fig. 21b, to excite modes that are not possible to excite from the halyard corners. The halyard-corner magnets (located near the mast tips) and the hypotenuse magnets were mounted on vertical translation stages, with linear actuators, to enable precise remote positioning of the magnets when testing in the vacuum environment. Because the magnets need to be positioned within 5 mm of the sail to work properly, small cameras were positioned next to each magnet and carefully aligned to validate that the proper gap size was achieved. To reduce sail motion during pumpdown of the vacuum chamber the mast tips were secured with an electromagnet, shown in Fig. 22a, which prevented vertical and lateral motion. During pumpdown of the vacuum chamber, a constant voltage was supplied to the mast-tip electromagnets to prevent motion due to air currents. Upon reaching a vacuum, the voltage to the electromagnet was removed, allowing the spring to pull the magnet away from the test article. The mast tips were then free to move with the soft suspension system off-loader, shown in Fig. 22b.

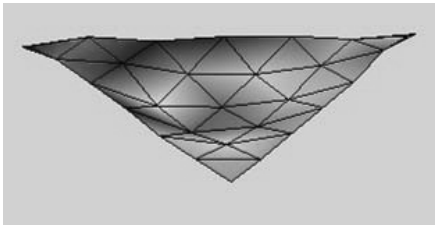

a) Mode 1: 1.11 Hz

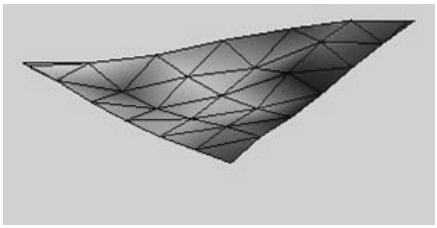

b) Mode 2: 1.19 Hz

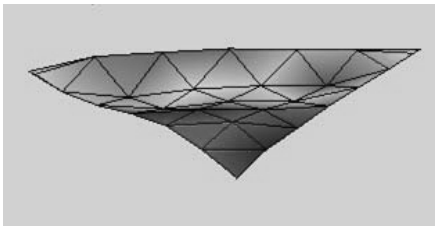

c) Mode 3: 1.50 Hz

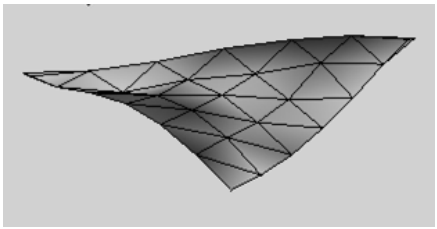

d) Mode 4: 1.72 Hz

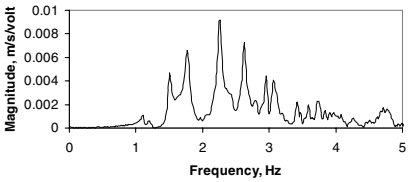

e) FRF

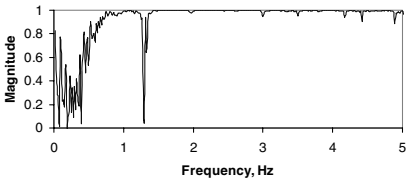

f) Coherence

Fig. 13 Dynamic response by magnetic excitation at tack line for 10-m sail component.

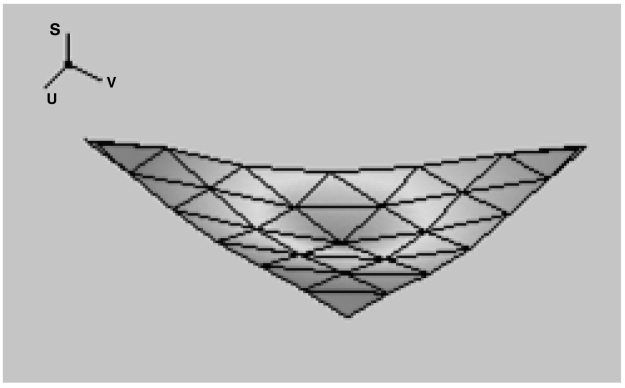

a) Mode 1: 1.47 Hz

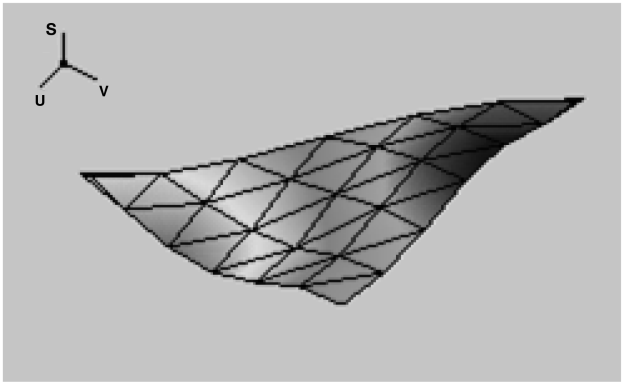

b) Mode 2: 1.94 Hz

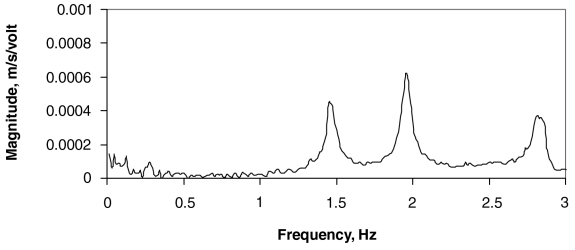

c) FRF

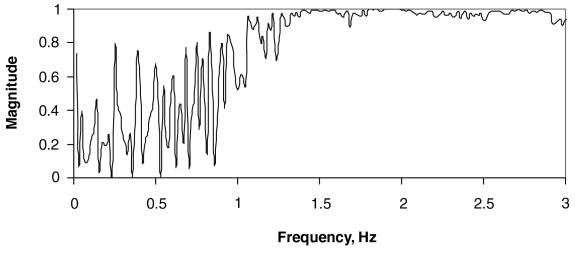

d) Coherence

Fig. 14 Dynamic response by MFC excitation at right angle of quadrant for 10-m sail component.

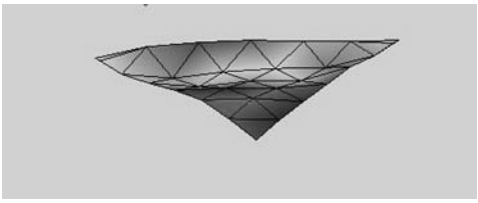

a) Mode 3: 1.53 Hz (MFCs actuated in-phase)

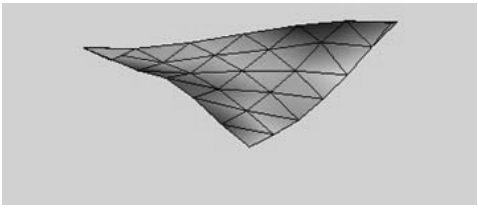

b) Mode 4: 1.84 Hz (MFCs actuated out-of-phase)

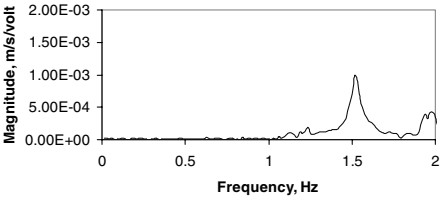

c) FRF when MFCs actuated in-phase

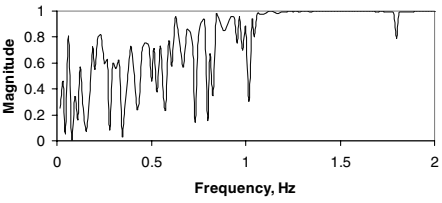

d) Coherence when MFCs actuated in-phase

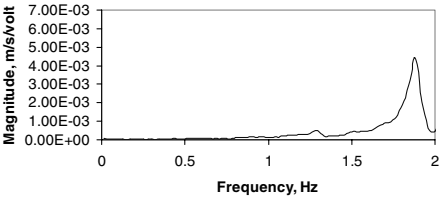

e) FRF when MFCs actuated out-of-phase

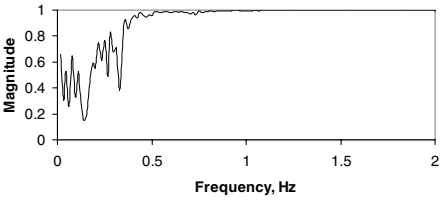

f) Coherence when MFCs actuated out-of-phase

Fig. 15 Dynamic response by MFC excitation at center of short cord for 10-m sail component.

The eight in-vacuum system-dynamics tests completed on the 20-m sail in the 0-deg spreader-bar configuration are summarized in Table 3. Most of the team's effort for this series of tests was focused on getting the best quality data possible on quadrant 4 (Q4), because this quadrant was the most pristine sail membrane, with few flaws, and it had flightlike characteristics, such as rip stops, built into the membrane. Quadrant 3 (Q3) was tested second with a reduced set of measurements because it was the next best quality quadrant with only some slight differences from quadrant 4, such as the lack of ripstops. Quadrants 2 (Q2) and 1 (Q1) were tested last with fewer measurements, because these quadrants were of least interest for model correlation. In particular, quadrant 2 had a major repair, whereas quadrant 1 had been used to develop and validate deployment methods and, as a result, had many wrinkles and small repairs. The quadrant tests were followed by a full-sail system test in a vacuum, in which one halyard-corner magnet (M1) on each quadrant was driven simultaneously and in-phase with a sine-wave sweep excitation. This technique allows for adequate excitation of the entire sail system and allows for the identification of major

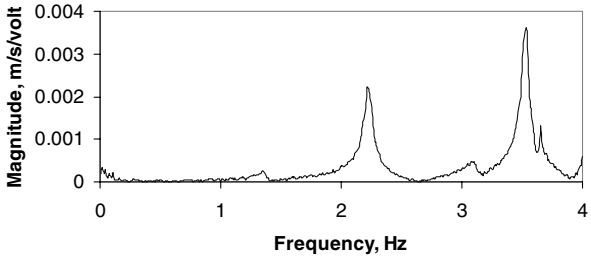

a) FRF

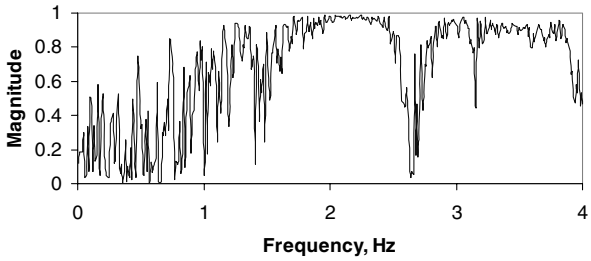

b) Coherence

Fig. 16 Dynamic-response by magnetic excitation at tack line for 10-m system.

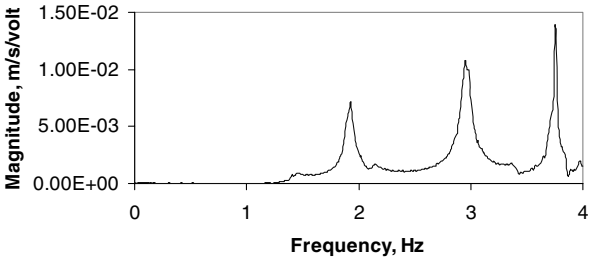

a) FRF

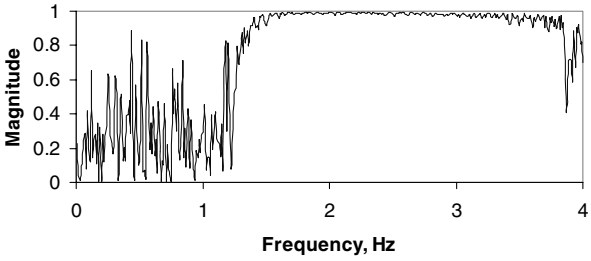

b) Coherence

Fig. 17 Dynamic response by magnetic excitation at halyard corner for 10-m system.

system-level vibration modes. To save test time, the full-sail system test only measured five sail-membrane locations per quadrant and two mast-tip measurements per mast. Because the test article configuration did not change going from the quadrant tests to full-sail system testing, the high spatial resolution quadrant-test results could be compared with the lower spatial resolution system-test results to make an assessment as to how the quadrants respond at each system-level mode.

During the chamber pumpdown process for the 20-m sailcraft, the sail sagged significantly (over 3 in.). It was discovered that this sag was caused by moisture buildup on the sail, which added weight to the sail. The Plum Brook vacuum chamber produces a large moisture buildup (fog) during pumpdown. The additional weight of the moisture on the sail caused the halyard negators to pay out the cord at

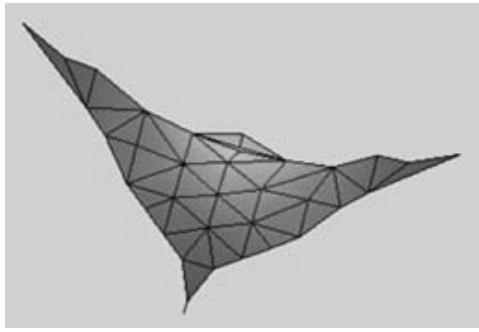

a) Mode 1: 1.40 Hz (corner excitation)

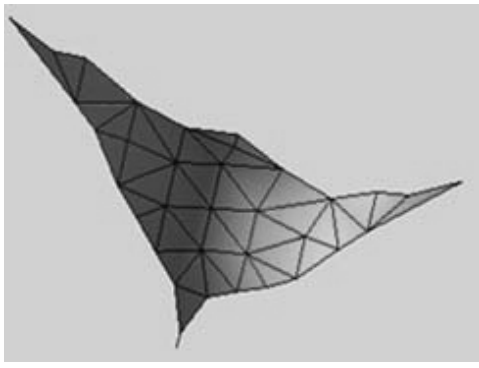

b) Mode 2: 1.82 Hz (corner excitation)

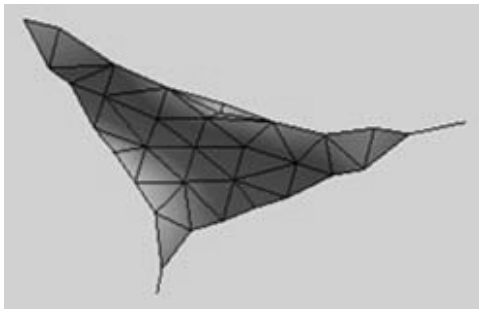

c) Mode 3: 2.23 Hz (from tack-line excitation)

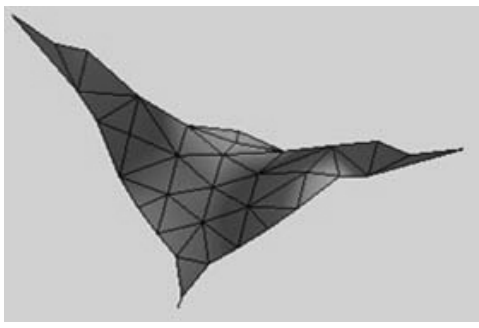

d) Mode 4: 2.82 Hz (corner excitation)

Fig. 18 Mode shapes from magnetic excitation testing for 10-m system.

the mast tips. The resulting sag at the center of the sail hypotenuse was large enough that the linear actuators could not reposition the magnets close enough (within 5 mm) to the sail for proper excitation. Because the magnets were mounted above the sails for this test, the only impact was that the magnets on the hypotenuse were useless for excitation, which limited testing to using only halyard-corner magnets for sail excitation. Ultimately, not being able to use the magnets at the hypotenuse limited the mode shapes that could be excited, which will be discussed later herein. All the tests used either

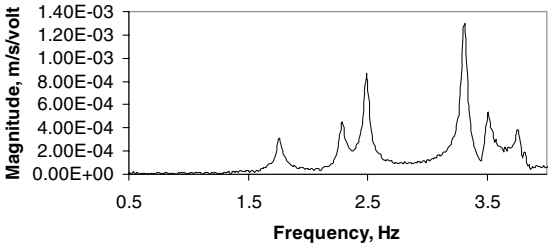

a) FRF

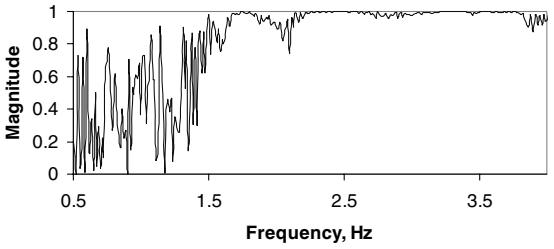

b) Coherence

Fig. 19 Dynamic response by a single MFC actuator at right angle of quadrant for 10-m system.

one or both remaining halyard magnets for sail excitation. All in-vacuum sail-system tests applied a sine-wave sweep input signal to the exciter, with a bandwidth from 0 to 3 Hz. The sine-wave sweep voltage signal was used as the reference value for the frequency response function (FRF) calculations, and the FRFs were computed using four averages. Analysis of the test data began by reviewing the FRFs from each quadrant test, and by identifying and listing all the resonant frequencies. Each of these modes where then categorized as to how well it was excited and identified in the FRFs. Modes with well-defined peaks in most FRFs were given a data quality rank of 1, or 1− for somewhat lower quality peaks. Modes with well-defined peaks, but closely coupled to other modes or in the residual of other modes as identified in the FRFs, were given a rank of 2, or 2− for modes of lower quality. Modes of potential interest that were in the frequency ranges of high modal density and perhaps significantly buried in residuals of other modes were ranked a 3. Only modes with a rank of 2+ or better that also repeated well for every quadrant test (with only minor frequency differences) were considered to be successfully obtained and marked as useful for analysis model correlation. Only the data from the quadrant 4 tests were used for model correlation. The other quadrant tests were performed primarily to determine the differences between the quadrants and their influence on the system-response behavior. Table 4 summarizes the dominant modes identified through this review process for the quadrant 4 tests. The table provides notes explaining whether each mode is a "mast dominate mode," meaning the sail primarily follows the motion of the mast, or a "sail dominate mode" were there is low mast participation in the response. The mode shapes are described based on the bending pattern along the long cord (hypotenuse) of the quadrant, and also down the quadrant centerline that extends from the tack-line corner (the quadrant 90-deg position) to the center of the quadrant hypotenuse. A first bending mode along the long cord means the long cord (hypotenuse) of the sail quadrant is undergoing bending with one inflection point along its length. Correspondingly, a centerline first bending mode would have one inflection point along its length down the centerline. Whereas, a centerline second bending mode would have two inflection points along its length down the quadrant centerline.

Mode 1, identified in Table 4 and Fig. 23a, was a dominant heavily damped mode with a damping factor of approximately 20%. This degree of damping is significantly higher than that exhibited by all the other modes, that have damping factors in the 2–3% range, and which is more typical of a structural mode of vibration. The high damping indicates mode 1 was a nonstructural mechanismlike mode,

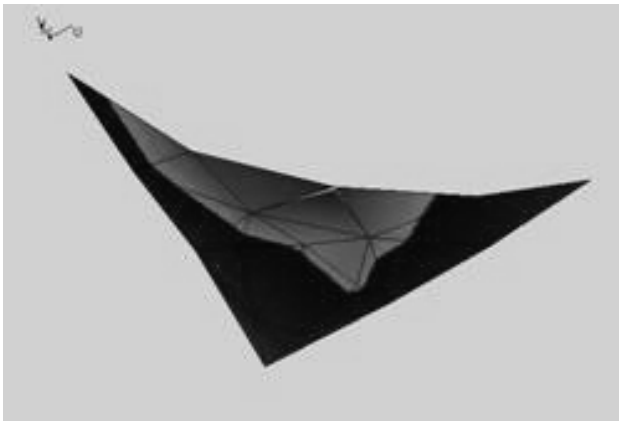

a) Mode 1: 1.78 Hz

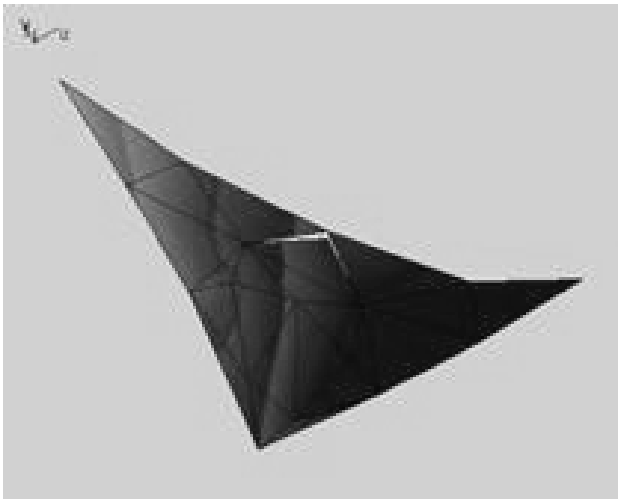

b) Mode 2: 2.30 Hz

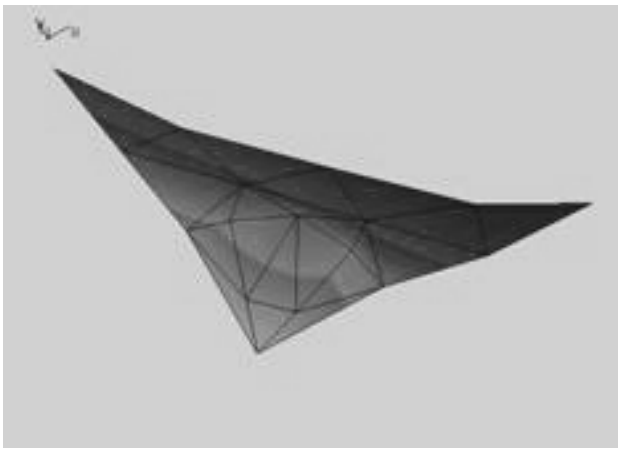

c) Mode 3: 2.50 Hz

Fig. 20 Mode shapes from a single MFC actuator at right angle of quadrant for 10-m system.

which may be caused by nonlinearities associated with free-play or sliding friction. Testing experience suggests that nonlinearities may have been introduced through the mechanism holding the system at the mast tips or through the negator springs attached to the sail-membrane cord. The mast tip was supported by negator springs that are left unlocked during testing to allow for mast-tip vertical motion to minimize dynamic interference with the sail system. The sail

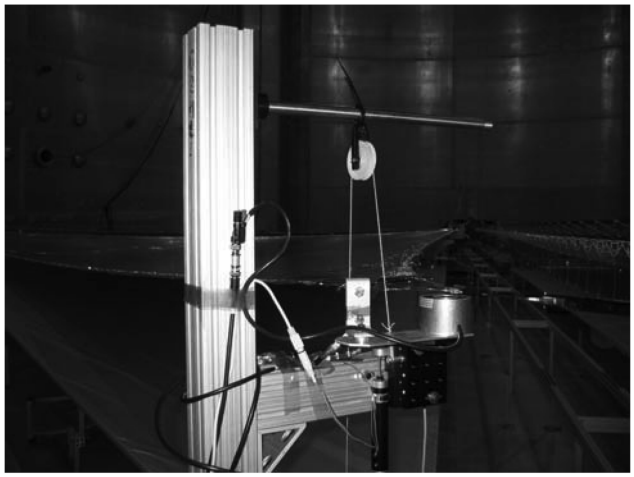

a) At halyard corner

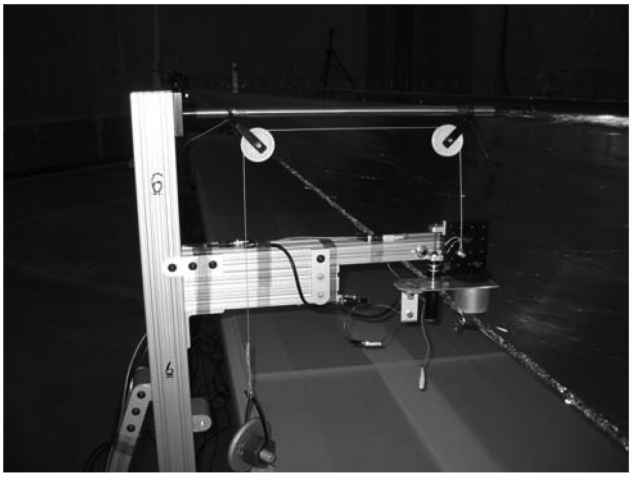

b) At quadrant hypotenuse position

Fig. 21 Magnetic exciter configuration for 20-m system.

membrane was also supported by negator springs at the mast-tip halyards that were designed to allow for constant loading during thermal expansion; however, the negator could also allow for cord sliding friction during dynamic excitation.

By comparing quadrant-test results with system-test results, it was found that modes 2, 3, and 7 were primarily mast-dominated modes with the sail motion following the mast tips. Mode 2 was the first full-system mode, where each sail membrane is rocking and pivoting about the quadrant centerline. Modes 4–6 and 8–9 were sail-membrane dominated modes. Mode 4 was a sail-membrane first breathing mode, with the long cord in first bending and the quadrant centerline also in first bending. The other sail-dominant modes were all in first bending along the long cord, but undergo various degrees of bending down the quadrant centerline starting with second bending for modes 5–6 and then to third bending for modes 8–9. Modes 1–4 and 7–9 were easily identified in all the quadrant test data. Modes 5 and 6 were strong well-defined modes in the FRFs for most tests, but were not consistently so for some. Figure 24 indicates that modes 5 and 6 on quadrant 4 could not be consistently excited from the halyard magnets. It turns out that this mode was difficult to excite from the halyard corners, because these locations were near a node line of the mode shape. The goal was to use the exciters at the quadrant hypotenuse for modes like these, but as mentioned previously the sail sag shifted the sail quadrant hypotenuse out of the range of the exciter. Thus, the sail sag limited the testing to using only halyard magnets. Another limitation found was that no second and third order modes on the hypotenuse could be excited with the halyard magnets being at the node line of these modes.

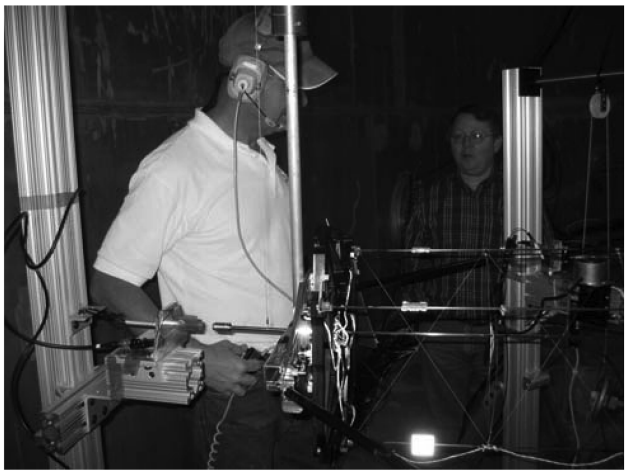

a) Magnetic restraint system

b) Soft suspension negator spring

Fig. 22 Mast tip off loaded with negator spring and fixed during pumpdown for 20-m system.

The full-sail system test (when all four quadrants were excited simultaneously) shows exceptionally strong mast participation for modes 2 and 7, as shown in Fig. 25. These are system-level mast-dominated modes with the sail membrane following the mast as shown by the mode shapes. Mode 2, the first fundamental system mode of the solar sail, is a "pinwheel mode" with all quadrants rocking in-phase. This mode has all mast tips twisting in-phase and the quadrants following the motion by rocking and pivoting about the quadrant centerline. Mode 7 is a mast-dominated mode in which the

Table 3 Magnetic excitation dynamic tests on 20-m system in vacuum

#	Test name	Meas. #
1	Q4 M1M2	44
2	Q4 M1	44
3	Q4 M2	44
4	Q3 M1M2	15
5	Q3 M1	15
6	Q1 M1M2	15
7	Q2 M1M2	13
8	Q1234 M1	28

Table 4 Magnetic excitation dynamic test results on quadrant 4 for 20-m system in vacuum

Summary of dominant modes				
#	Hz	Rating	Description	Notes
1	0.391	1	Sail vertical motion/heavily damped nonlinear mechanism mode	Potentially related to negator springs in halyard and on mast tip
2	0.503	1	Sail system first mode "pinwheel mode" sail rocking/all mast tips twist in-phase	Mast dominant mode, sail follows
3	0.625	1−	Sail rocking/*y* tips out of phase/*z* tips out of phase	Mast dominant mode, sail follows
4	0.687	2+	Sail-membrane first breathing mode long cord first bending/centerline first bending	Membrane mode, first centerline
5	0.937	2+	Long cord first bending/centerline second bending (1)	Membrane mode, second centerline
6	1.00	2+	Long cord first bending/centerline second bending (2)	Membrane mode, second centerline
7	1.06	1	Asymmetric sail mode left side short cord and right side long cord out of phase	Mast dominant mode, sail flex, full system response
8	1.41	1−	Long cord first bending/centerline third bending (1)	Membrane mode, third centerline
9	1.47	2+	Long cord first bending/centerline third bending (2)	Membrane mode, third centerline

sail membrane bends asymmetrically. In this asymmetric bending mode, the mast tips twist out of phase with one another at each quadrant halyard corner.

IV. Static Shape Testing with Photogrammetry

A. Measurement Method

A static shape test was conducted on the 10-m system in the 16-m vacuum chamber at LaRC. Figure 26 shows this 10-m solar–sail quadrant deployed inside the chamber. For the photogrammetry test, a total of 31 one-inch retroreflective circular targets were distributed on the sail in a uniform grid pattern. Additionally, multiple retroreflective targets were mounted on the rigid framework supporting the sail and also on the surrounding floor area. The photograph in Fig. 26 is taken with the facility lights turned on, which illuminates the entire test article and some of the photogrammetry targets on the membrane and the surrounding structure. However, turning the facility lights off and illuminating the sail with lights near the photogrammetry cameras allow for much easier identification of the photogrammetry targets for static shape testing purposes.

The photogrammetry camera locations inside the test chamber are shown in Fig. 27. Each camera was installed in a pressurized canister mounted onto a pan-tilt unit that could be controlled from outside the chamber by an operator. The operator could also adjust the zoom lens, iris, and focus settings for each camera remotely from the control room of the facility. The camera support brackets were bolted to edges of the catwalk, approximately 35 ft above the chamber floor. This camera geometry provided light-ray intersection angles of approximately 60 deg in each direction. The cameras were able to image the entire sail quadrant without being repositioned. The average measurement precision obtained for each point was 0.017, 0.017, and 0.22 in. in the *x*, *y*, and *z* axis, respectively.

To meet the need for full-field measurement of highly flexible, large gossamer structures such as solar sails, LaRC personnel developed a multicamera, high-resolution, digital imaging and recording system. The system records up to six synchronized, 2-megapixel digital video cameras operating at frame rates up to 30 fps (frames per second). Each camera has a motorized zoom lens with focal length settings of 16–160 mm. All imagery from the cameras was streamed in uncompressed digital form onto an array of high-speed disks.

The internal components of each camera canister are shown in Fig. 28. The environmental constraints of working in a vacuum presented the biggest challenge. The factors considered the most challenging were pressure and temperature, camera-to-computer communication, and lighting. The thermal sensitivity of the camera from self-heating in this environment was a primary concern. To alleviate this problem, the cameras were packaged in pressurized canisters with a regulated purge-air supply to maintain stable temperatures and airflow. The working distance from the cameras to the data acquisition computer exceeded the limits for proper data communications over copper wire. Therefore, to support data communications over long distances, optical converters were added to the design to transfer all images digitally over fiber optic cables. Lighting requirements for target illumination were driven by the use of retroreflective measurement targets. Optimal photogrammetric centroiding accuracy with retroreflective targets requires concentric lighting at the camera. To satisfy this requirement and the effects of a vacuum environment, a custom high-intensity light-emitting-diode (LED) array was assembled for each camera package. This ring light was installed at the end of each canister, encircling the camera lens. The LED light intensity and all internal camera settings such as integration time could also be adjusted remotely from the control room of the facility.

Figure 1d shows the ATK 20-m solar sail deployed inside the Plum Brook vacuum chamber. For the photogrammetry shape-measurement test, approximately 250 one-inch retroreflective circular targets were distributed on the sail in a uniform grid pattern. In addition, high-precision scale bars with two-inch targets were positioned along the perimeter of each quadrant. The scale bars served as the primary standard by which all measurements were based. An example of the scale bar is shown in Fig. 29.

The same camera packages used for the 10-m sail quadrant test were used in the shape testing of the 20-m sail in the Plum Brook vacuum chamber. These camera packages were rigidly mounted near the top corners of the doors in the large assembly area. Each camera imaged the sail from a position approximately 55 ft above the chamber floor, and an additional fifth camera was located on the overhead crane platform approximately 120 ft above the chamber floor. The camera arrangement is depicted in the graphic shown in Fig. 30. The size of the sail and the distance to the cameras required the 20-m sail test to be measured in a piecewise manner. Each camera in use was repositioned during the image acquisition process to ensure full sail coverage. Each of the five cameras recorded nine images to achieve the full coverage needed to compute the shape-measurement solution. The images were recorded in the acquisition sequence depicted in Fig. 31.

B. Shape Results and Discussion

During the shape testing of the 10-m sail, the images used for photogrammetry were purposely underexposed to simplify locating the illuminated targets and determining their centroid. However, the lack of most background information in the images can make it difficult to identify specific targets during data analysis. Therefore, during test setup, several additional retroreflective targets were placed around the perimeter of the sail for visual reference and scaling purposes. These additional targets are also useful during comparison of different data sets (for example, the data sets acquired under different load conditions) because they are stationary points whereas the sail targets can change their three-dimensional locations somewhat with test conditions. These stationary targets were used for scaling and also provided three-dimensional reference points, which improves photogrammetric data analysis accuracy. Photogrammetry data were acquired at ambient test conditions for each of three load conditions. Static loads of 1.5, 2.5, and 3.5 lb were applied through

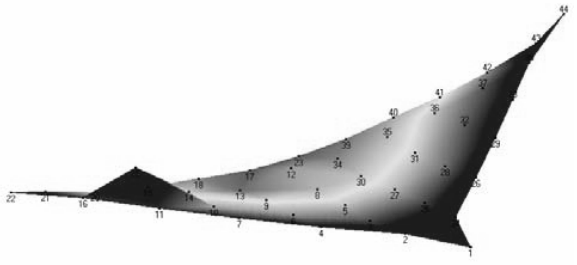

a) Mode 1: 0.391 Hz

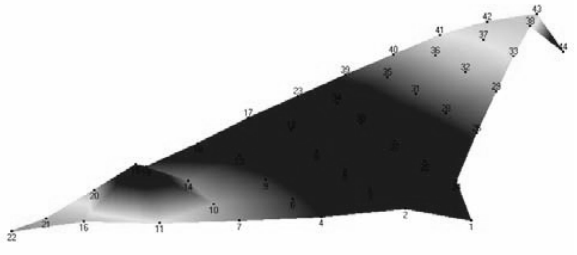

b) Mode 2: 0.503 Hz

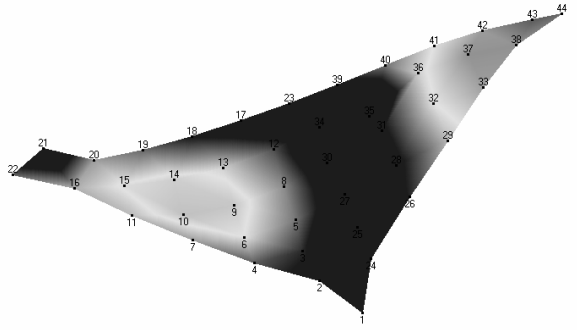

c) Mode 3: 0.625 Hz

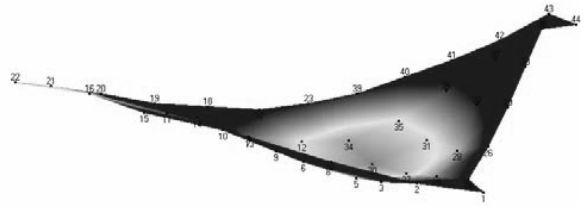

d) Mode 4: 0.687 Hz

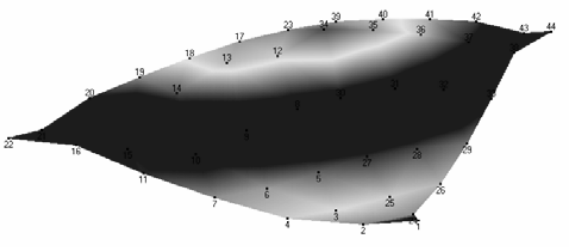

e) Mode 5: 0.937 Hz

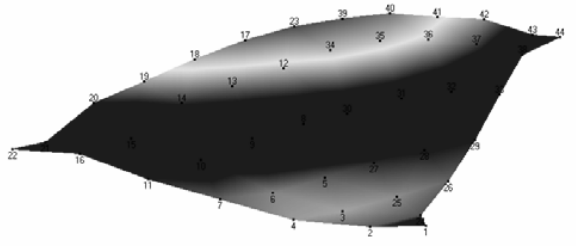

f) Mode 6: 1.0 Hz

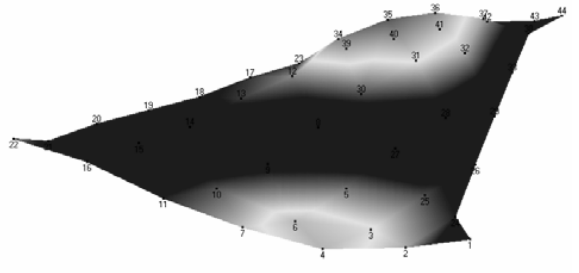

g) Mode 7: 1.06 Hz

h) Mode 8: 1.41 Hz

i) Mode 9: 1.47 Hz

Fig. 23 Summary of dominant operating deflection shape (ODS) modes from magnetic exciter tests on 20-m system.

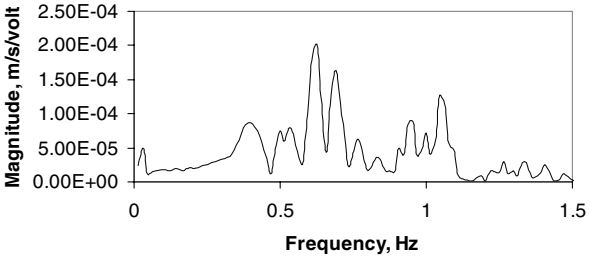

a) FRF M2 exciter (Q4M2)

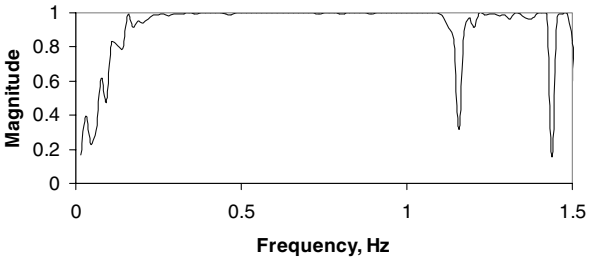

b) Coherence M2 exciter (Q4M2)

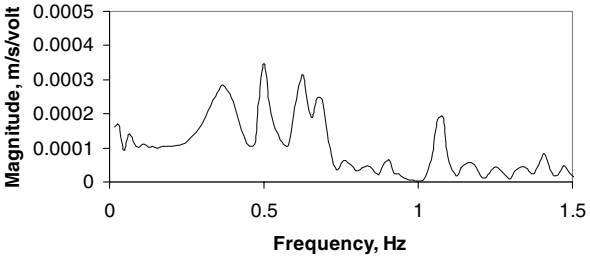

c) FRF M1 exciter (Q4M1)

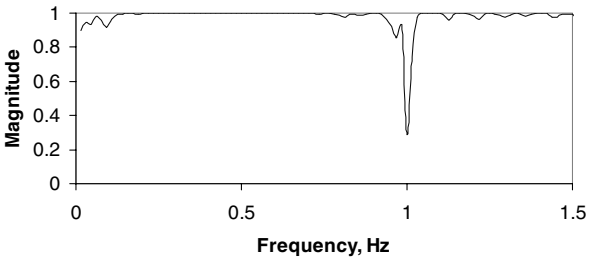

d) Coherence M1 exciter (Q4M1)

Fig. 24 Dynamic response measurement comparison M1 versus M2 magnetic exciter on 20-m system.

the tack line. Sail shape data representing the change in position of the 31 sail points for the 1.5, 2.5, and 3.5-lb load test were obtained photogrammetrically. The results displayed as displacement vectors for the 1.5-lb case are shown in Fig. 32. The 1.5-lb load test resulted in the largest out-of-plane displacement, where a maximum displacement of 6.46 in. was identified relative to the corner targets. The maximum displacements for the 2.5 and 3.5-lb loads were 4.73 and 4.13 in., respectively.

To verify the camera locations would provide adequate coverage and measurement precision for the 20-m sail, numerical simulations were performed before testing. The simulation showed it necessary to measure the 20-m sail in segments. Additionally, the simulations provided estimates of measurement precision. The predicted root-mean-square measurement precision was approximately 0.5 mm for the 20-m sail. Camera parameters such as pixel size and number of pixels on the camera were obtained from manufacturer specifications, and camera coordinates were derived from facility drawings.

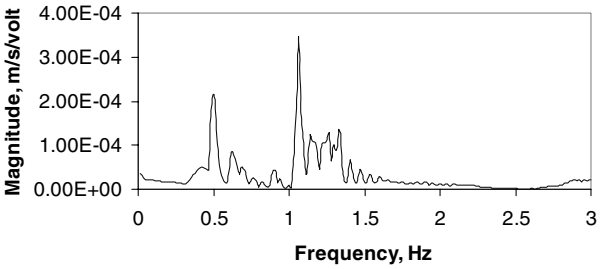

a) FRF for 20-m system dynamic response

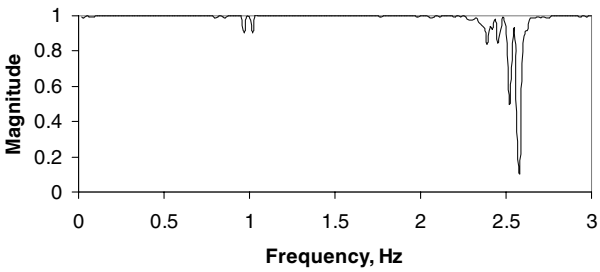

b) Coherence for 20-m system dynamic response

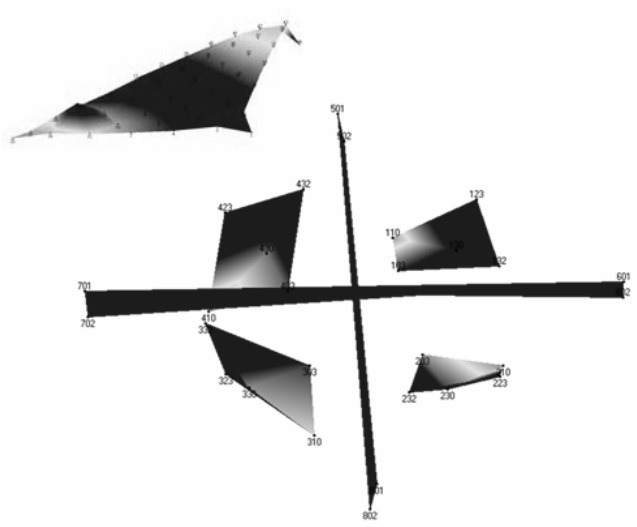

c) 0.5 Hz Mast dominant mode

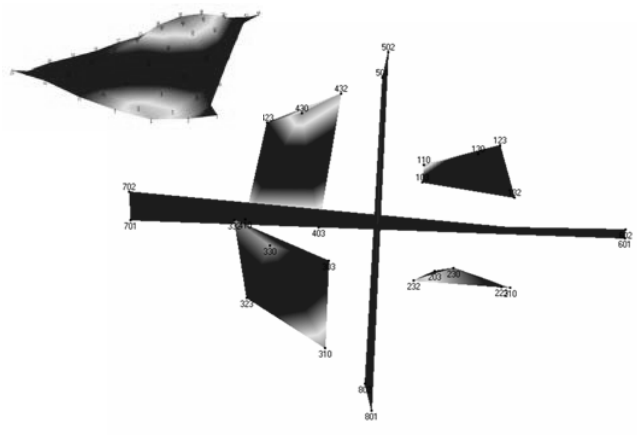

d) 1.06 Hz Mast dominant mode

Fig. 25 Dynamic response when all four quadrants excited simultaneously on the 20-m system (one magnetic exciter per quadrant).

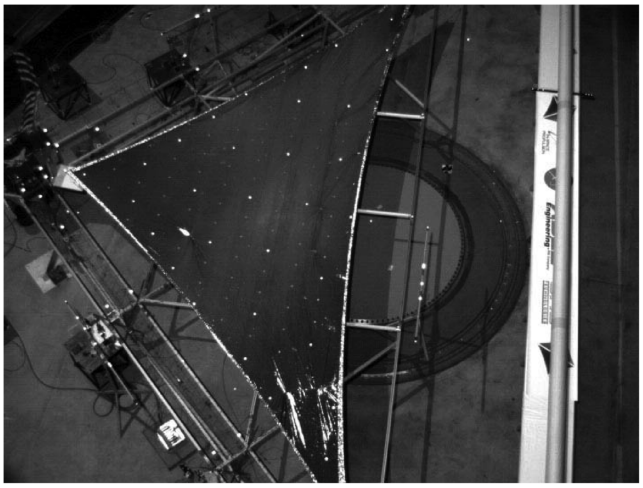

Fig. 26 10-m system in NASA-LaRC 16 m vacuum chamber as seen from photogrammetry camera 2.

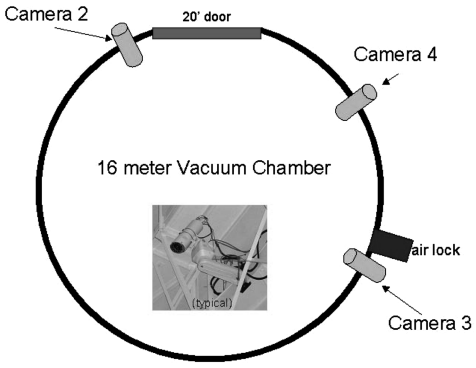

Fig. 27 Photogrammetry camera locations in NASA-LaRC 16-M vacuum chamber.

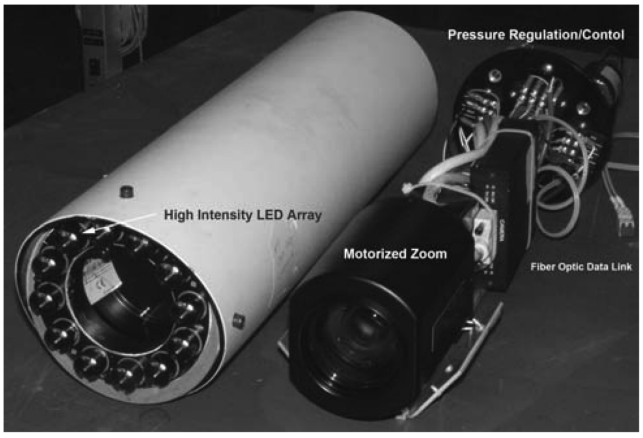

Fig. 28 Pressurized photogrammetry camera canister.

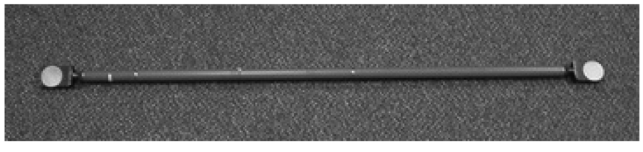

Fig. 29 Scale bar with 2-in. retroreflective end targets (typical).

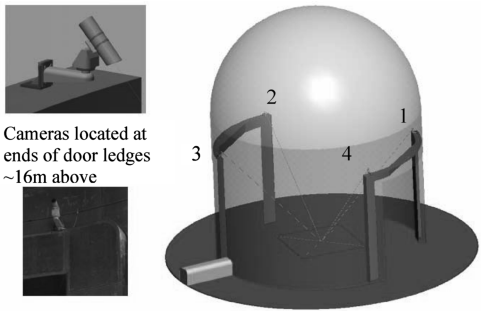

Fig. 30 Photogrammetry camera locations in Plum Brook vacuum chamber for 20-m system test.

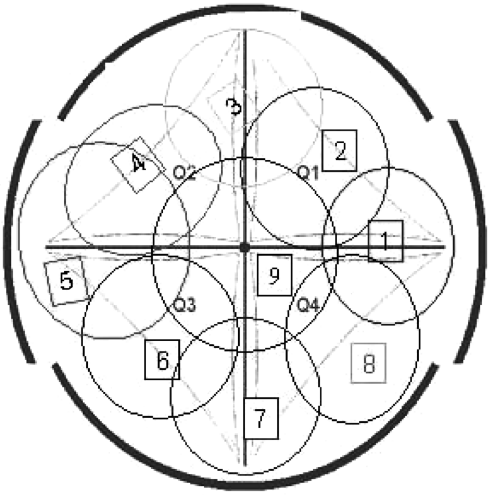

Fig. 31 Image acquisition sequence used by each of five cameras for 20-m system static shape measurement.

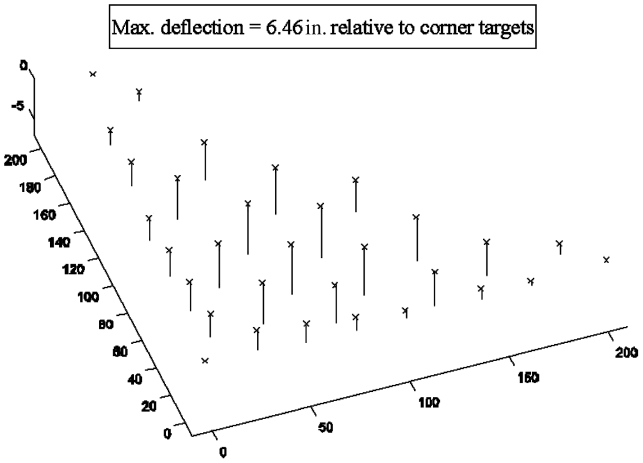

Fig. 32 Displacement results for 1.5-lb load test for 10-m system.

Figures 33a and 33b are images recorded for the 20-m sail from two of the door-camera positions. Figures 33c and 33d are correlated images created from the pretest simulation and used to predict overall precision of the camera configuration. During the static measurement, the chamber lights were turned off and the canister LED ring lights were activated to illuminate the grid of measurement targets. Qualitative comparison of the images shows excellent correlation of pre-test-simulation images with those recorded by the actual measurement.

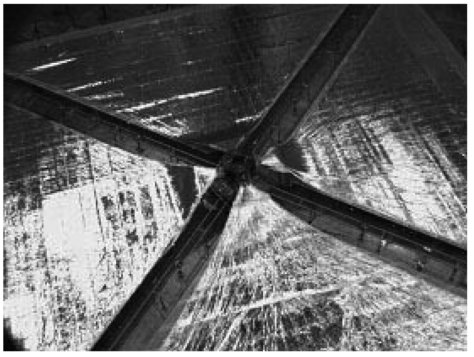

a) Camera 1 photo

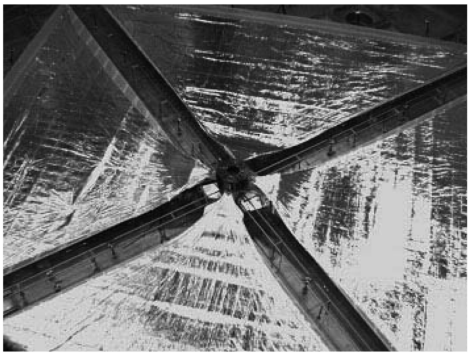

b) Camera 2 photo

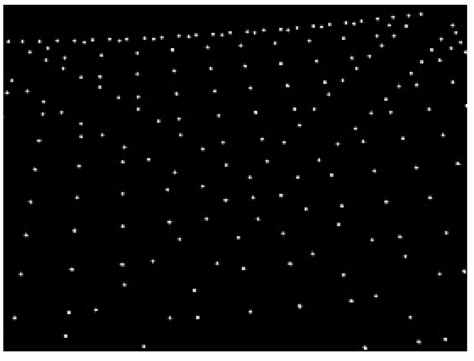

c) Camera 1 simulation

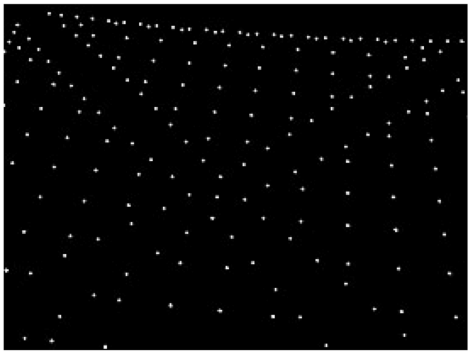

d) Camera 2 simulation

Fig. 33 Image correlation between pretest simulation and actual camera configuration for 20-m system.

Simulation of the 20-m sail indicated that the lowest-precision measurements would occur in the boom tip area under the large access doors. The lower precision is attributed to the somewhat restricted view and poor convergence angle of the imaging cameras to the sail in these areas. In each case, the area in question is visible to

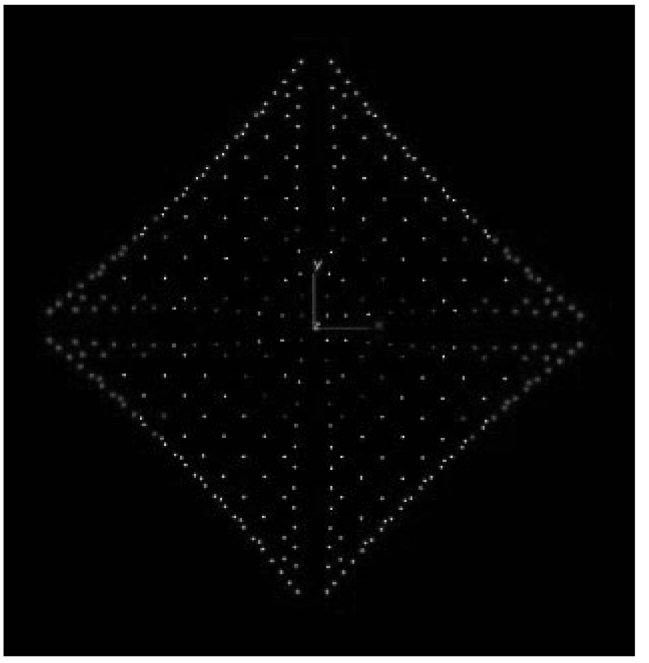

Fig. 34 20-m system with error ellipsoids (dark gray) predicted through simulation to determine precision error.

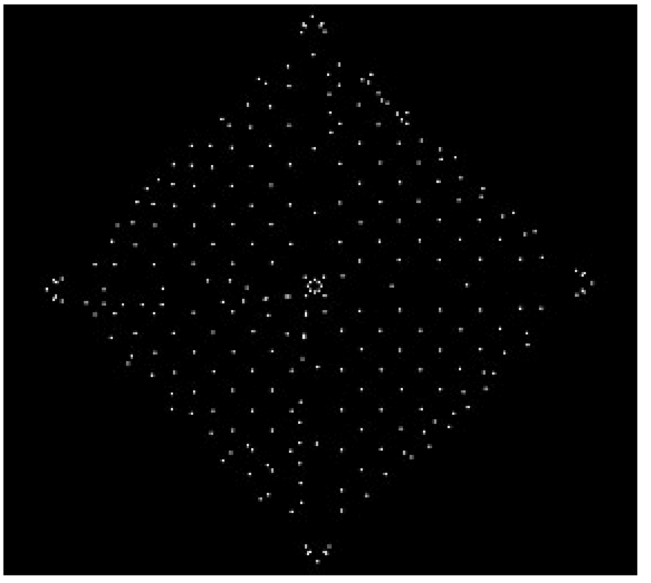

Fig. 35 Three-dimensional point cloud of 20-m system targets.

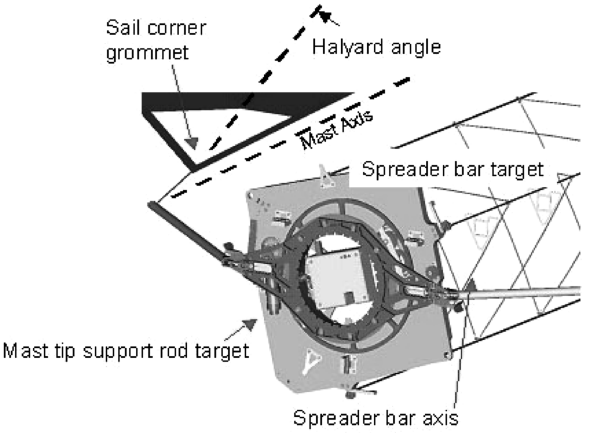

Fig. 36 Halyard line angle setting at mast tip for 20-m system.

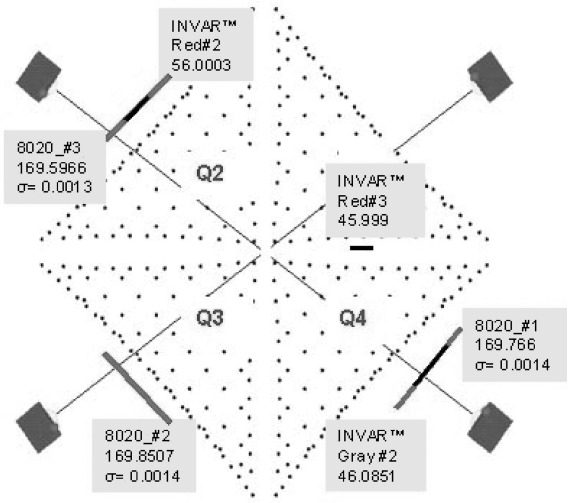

Fig. 37 Scale bar locations relative to 20-m system.

three of the five cameras. The diagram in Fig. 34 represents the lower-precision areas with "error" ellipsoids that have a relative scale in proportion to the predicted precision.

To automate the image processing task in this test, additional retroreflective coded targets were added around the perimeter of the sail. These coded targets were unique identifiers, recognizable to the processing algorithm that was used to help determine sail orientation. For the 20-m sail, the photogrammetry data were acquired at ambient conditions. The chamber was isolated with all access and venting points secured 20 min before the test to allow the sail to reach a steady state condition. The results for the full-field static shape measurements were successfully obtained. The shape measurements were performed for three sail configurations that include halyard angles of 0, 22.5, and 45 deg. A three-dimensional point cloud representing the photogrammetry results obtained for the 20-m sail in ambient condition is shown in Fig. 35. The data are for the 0-deg halyard angle. A graphic outlining the halyard angle setting is shown in Fig. 36. The static shape measurement included more than 250 targets, 26 of which were scale and reference points around the perimeter of the sail. Similar results were recorded for the halyard angle settings of 22.5 and 45 deg.

To validate the accuracy of the overall measurement, "scale points" of known dimension were placed along the perimeter of the four quadrants. Their general location with respect to the sail is shown in Fig. 37. To predict the overall accuracy of the sail measurements, the known value of each scale point was compared with its measured value determined by the photogrammetric processing. The differences ranged from 0 to 0.033 in., with a mean value of 0.011 in. Table 5 summarizes the results.

A plot of the estimated precision for the derived three-dimensional coordinates of each point as part of the halyard 0-deg angle case is provided in Fig. 38. The coordinate system was established with the x axis being out of plane. The mean value for the x-axis displacement is approximately 0.02 in. Notably, the principal outliers shown in the plot correspond to points lying along the edges or mast-tip areas where low precision was predicted by the simulation.

Table 5 Three-dimensional point validation checks using known scale points

Quad location	Type	Known, in.	Measured, in.	Delta, in.
Q1/Q4	INVAR R#3	45.999	46.9690	−0.0001
Q2	INVAR R#2	56.0003	55.9953	−0.0060
Q4	INVAR G#2	46.0851	46.0750	−0.0100
Q4	80/20 #1	169.766	169.7663	0.0000
Q3	80/20 #2	169.851	169.9233	0.0726
Q2	80/20 #3	169.597	169.6290	0.0324

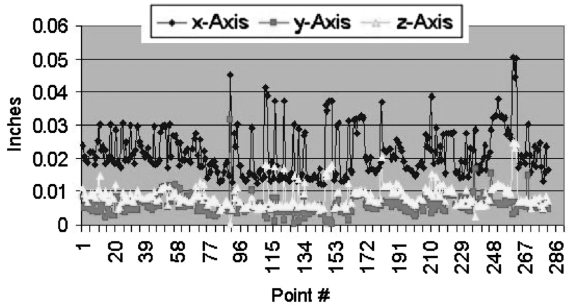

Fig. 38 Point precisions for 0-deg halyard angle on 20-m system showing outliers near mast-tip area as predicted.

V. Conclusions

Overall the photogrammetry tests on the 10- and 20-m sails are considered a success. All of the cameras, canisters, and image recording hardware operated flawlessly and provided quality imagery for both the photogrammetry analyses and also for documenting sail deployment. By using a darkened test chamber and adjusting the variable-intensity LED ring lights on the camera canisters as needed, all photogrammetry images had high contrast between the retroreflective targets and the dark image background. All images were processed with commercial software, without undue difficulty, and provided three-dimensional experimental results useful for correlation with analytical models.

The results of the present study indicate that for the sail-only dynamics tests, surface-bonded piezoelectric patches can be used to successfully perform modal tests on a quadrant of a large-area ultralightweight solar-sail membrane in a vacuum. The tests were able to properly identify the first four modes, which is important for model correlation activity. It was found that piezoelectric actuators could also be used to characterize the modal behavior of a built-up EDU mast structure. For both cases, the results obtained by using piezoelectric actuators were compared with results obtained by using other, more traditional techniques as a check of the consistency between the two techniques. Although the magnetic exciter and impact-hammer methods have an advantage in performing structural dynamic identification on large ultralightweight gossamer structures, such as solar sails, due to their noncontacting nature, these methods could not be used in future planned flight test programs for on-orbit validation. Only during on-orbit validation can these structures be properly characterized, in an environment free of the effects of gravity. The piezoelectric patches offer a very attractive approach for on-orbit dynamic-response validation of gossamer structures because they are light weight, can be manufactured in many diverse ways, and can be configured to be embedded in the structure.

A 10-m sail quadrant has been tested to determine its in-vacuum, system dynamic response for correlation of analysis models that are to be used to aid in future design efforts for potential flight missions. The sail has been shown to respond in a predictable manner, and the test results have been found to be reliable and useful for model correlation. Several test techniques were examined and have been refined, and potential on-orbit test methods have been identified for further investigation for a flight validation mission.

The 20-m solar–sail dynamics test program performed at the Plum Brook vacuum chamber facility was successfully completed, with all test requirements met on time and schedule. Most important, the fundamental sail-system modes needed for analysis model correlation were identified. In addition, higher-order sail-membrane modes were identified through a combination of many tests on each quadrant of the sail. The fundamental modes of the mast, critical for model correlation, were also identified using an innovative excitation technique that is suitable for flight testing. Also, various excitation techniques were evaluated for in-vacuum dynamic-response tests. These techniques were shown to have promise, and recommendations for further study have been made for incorporation into future test programs.

Acknowledgments

The work described in this paper was funded by the In-Space Propulsion Technology Program, which is managed by the NASA's Science Mission Directorate in Washington, D.C., and implemented by the In-Space Propulsion Technology Office at the Marshall Space Flight Center in Huntsville, Alabama.

References

[1] Montgomery, E., and Johnson, L., "Development of Solar Sail Propulsion for NASA Science Missions to the Inner Solar System," AIAA Paper 2004-1506, 2004.

[2] "The Sun-Earth Connection Roadmap 2003–2028: Understanding the Sun, Heliosphere, and Planetary Environments as a Single Connected System," NASA NP-2002-8-500-GSFC, 2002.

[3] Murphy, D., Murphey, T., and Gierow, P., "Scalable Solar–Sail Subsystem Design Concept," *Journal of Spacecraft and Rockets*, Vol. 40, No. 4, 2003, pp. 539–547.

[4] Murphy, D., Trautt, T., McEachen, M., Messner, D., Laue, G., and Gierow, P., "Progress and Plans for System Demonstration of a Scalable Square Solar Sail," American Astronautical Society Paper 04-105, 2004.

[5] Gaspar, J. L., Mann, T., Behun, V., Wilkie, W. K., and Pappa, R., "Development of Modal Test Techniques for Validation of a Solar Sail Design," AIAA Paper 2004-1665, 2004.

[6] Murphy, D., Macy, B., and Gaspar, J., "Demonstration of a 10 m Solar Sail System," AIAA Paper 2004-1576, 2004.

[7] Gaspar, J. L., Behun, V., Mann, T., Macy, B., and Murphy, D., "Testing of a 10 Meter Quadrant Solar Sail," *Proceedings of the 24th International Modal Analysis Conference*, Society for Experimental Mechanics, Bethel, CT, 2006.

[8] Murphy, D., Macy, B., and Gaspar, J., "Demonstration of a 20 m Solar Sail System," AIAA Paper 2005-2126, 2005.

[9] Gaspar, J., Behun, V., Mann, T., Murphy, D., and Macy, B., "Testing of a 20-Meter Solar Sail System," *53rd JANNAF Propulsion Meeting*, Johns Hopkins Univ. Chemical Propulsion Information Agency, Columbia, MD, 2005.

[10] Murphy, D., "Validation of a Scalable Solar Sailcraft," *53rd JANNAF Propulsion Meeting/2nd Liquid Propulsion Subcommittee/Spacecraft Propulsion Subcommittee Joint Meeting*, Johns Hopkins Univ. Chemical Propulsion Information Agency, Columbia, MD, 2005.

[11] Taleghani, B. K., Lively, P. S., Banik, J., Murphy, D. M., and Trautt, T. A., "20 Meter Solar Sail Analysis and Correlation," *53rd JANNAF Propulsion Meeting/2nd Liquid Propulsion Subcommittee/Spacecraft Propulsion Subcommittee Joint Meeting*, Johns Hopkins Univ. Chemical Propulsion Information Agency, Columbia, MD, 2005.

[12] Slade, K. N., Belvin, W. K., and Tetlow, T. K., AIAA Paper 2003-1744, 2003.

[13] Wilkie, W., Bryant, R., High, J., Fox, R., Hellbaum, R., Jalink, A., Jr., Little, B., and Mirick, P., "Low-Cost Piezocomposite Actuator for Structural Control Applications," *Society of Photo-Optical Instrumentation Engineers 7th Annual International Symposium on Smart Structures and Materials*, International Society for Optical Engineering, Bellingham, WA, 2000.

M. Nemeth
Associate Editor